2023년 2월

박사학위 논문

CMG기반 무인기 자세제어 안정화 기법 연구

조선대학교 대학원

항공우주공학과

양 유 영

CMG기반 무인기 자세제어 안정화 기법 연구

Attitude Control of UAVs Using Control Moment Gyros

2023년 2월 24일

조선대학교 대학원

항공우주공학과

양 유 영

CMG기반 무인기 자세제어 안정화 기법 연구

지도교수 이 현 재

이 논문을 공학 박사학위 신청 논문으로 제출함

2022년 10월

조선대학교 대학원

항공우주공학과

양 유 영

양유영의 박사학위논문을 인준함

위원장 조선대학교 교수 김 태 규 (인)

위 원 조선대학교 교수 이 현 재 (인)

위 원 조선대학교 교수 정 성 훈 (인)

위 원 조선대학교 교수 박 의 종 (인)

위 원 모아소프트 본부장 이 광 현 (인)

2023년 1월

조선대학교 대학원

목차

초 록

CMG기반 무인기 자세제어 안정화 기법 연구

양유영
지도교수 : 이 현 재
항공우주공학과
조선대학교 대학원

멀티로터는 사람을 대체하여 다양한 임무에 활용되고 있다. 원활한 임무 수행을 위해서 안정성과 신뢰성이 중요하다. 멀티로터는 풍속의 변화와 같은 외란에 멀티로터의 로터만으로 속도 제어를 통해 비행 안정성의 보장이 어렵다. 이를 해결하기 위해 외란에 강인한 제어기법을 이용하는 연구가 많이 이루어져 왔다.

바람과 같은 외란이나 모델의 불확실성을 해결하기 위해 외란에 강인한 제어기법인 슬라이딩 모드 제어를 사용하였다. 이 제어기법은 외란과 불확실성에 강인한 특징이 있지만 채터링(Chattering) 문제가 있으며 상태 오차가 0으로 수렴하기 위해 무한한 시간이 걸린다는 단점이 있다. 이를 해결하기 위해 자세 제어에는 Fast Terminal Sliding Mode Control과 고도 제어에는 Terminal Sliding Mode Control를 적용하였다.

외란으로 인해 자세가 틀어졌을 때 멀티로터의 모터 힘으로 자세를 안정시키기 어려움이 있어 빠른 반응속도를 위해 자이로스코픽 효과를 이용해 토크를 생성하는 장치인 Control Moment Gyro(CMG)를 활용하였다. CMG는 작은 입력으로 큰 토크를 발생시킬 수 있다는 장점을 가지고 있으며, 주로 고기동의 인공위성 자세제어에 사용된다. 인공위성에 국한되지 않고 선박과 차량 등 다양한 분야에 적용하여 연구가가 이루어지고 있으며, 최근 멀티로터 시스템으로 CMG와 반작용 휠을 사용하여 타당성 연구가 수행되었다.

CMG 휠의 회전속도으 변화성에 따라 크게 2가지 종류로 구분할 수 있다. 휠의 회전속도와 김벌의 각도를 조절하는 Variable Speed CMG(VSCMG)와 휠의 회전속도를 일정하게 유지하고 김벌의 각도를 조절하는 Constant Speed CMG(CSCMG)으로 구분할 수 있다. 본 논문에서는

CSCMG를 사용하였으며, 2개의 CMG를 동체 좌표계에서 X축에 나란히 부착한 형태를 사용하였다. 이 형태는 Roll과 Pitch 운동에만 관여하며 Yaw 운동에 관여하지 않는다. 이 형태를 사용한 이유는 Yaw 운동의 경우 멀티로터의 Z축 관성모멘트가 다른 축에 비해 커서 상대적으로 외란에 덜 민감하기 때문이다.

본 논문에서는 더 높은 추력과 세밀한 제어가 가능한 헥사로터를 사용하였으며, 설계한 시스템이 외란이 존재하는 환경에서 CMG가 장착한 헥사로터와 CMG를 장착하지 않은 헥사로터의 수치 시뮬레이션을 통해 제안한 알고리즘의 성능을 검증한다.

I. Introduction

Unmanned aerial vehicle (UAV) is largely classified into a fixed wing type and a rotary wing type according to the shape of the aircraft, and recently, a multi-rotor, one of the types of rotary blades, has been most actively studied. The multi-rotor has the advantage of being able to vertical take-off and landing (VTOL) and hovering in place through thrust control of each rotor, so it replaces human resources and performs missions such as monitoring, reconnaissance, target recovery, and damage evaluation for military purposes[1–3]. Recently, various tasks such as aerial photography, environmental monitoring, building inspection, and disaster management support have been performed in the private sector[4, 5]. As the use of multi-rotors increases, related accidents are also increasing every year around the world. Among them, the proportion of crashes and crashes is the highest, and most of them are problems that occur during flight[6, 7]. Commercial multi-rotors are specified to ensure flight stability at wind speeds of about 10 m/s. However, it is difficult to guarantee the flight stability of the multi-rotor even with slight changes in wind speed during actual flight. Although the multi-rotor is simple to model the system, it is difficult to ensure flight stability through speed control alone when there is disturbance such as rapid change in wind speed due to the relatively small and light aircraft, and the system and mathematical modeling of the actual model may be somewhat erratic, resulting in model uncertainty. The stability and reliability of the system must be ensured for smooth and safe mission performance. To solve these problems, research on robust control techniques for disturbance and uncertainty and nonlinearity of models is underway[8–10].

Typical nonlinear model control techniques for ensuring flight stability and reliability of UAVs include sliding mode control (SMC), backstepping control, neural network control, and adaptive control. Backstepping control is systematic in the design process of the control input and can be applied to systems with known nonlinearity that do not satisfy matching conditions, but it needs to know the nonlinearity of the system accurately and can cause rapid output changes[11]. Neural network control is a technique of setting variables related to a control model and setting the combination and weight of the model and variable as variables[12]. This technique is difficult

to design an intermediate layer that determines the weight, and as the number of layers increases, the control precision increases, but the amount of computation increases, requiring a lot of computation time. Adaptive control has model-based adaptive control and non-model-based adaptive control methods, which require a lot of computation for nonlinear models, and the more complex the model, the more difficult it is to apply.

Most of the control techniques introduced above have limitations in modeling nonlinear dynamics and handling various environmental variables, and it is expected that accurate and quick response to perform tasks in situations of disturbance and model uncertainty will be difficult. Sliding mode control, which follows the target state accurately and quickly and is robust to disturbance and model uncertainty, can handle nonlinear dynamics without linearization, define a sliding surface using system state variables, and control variables to make the system behave[13]. However, sliding mode control has two problems. First, chattering, a high-frequency shaking phenomenon, occurs in the process of increasing robustness. Second, it takes infinite time for the state error to converge to zero[14, 15]. Such a problem can lead to a decrease in control performance, and research has been conducted to improve it. A method of improving and using the problem-causing Reaching law to reduce chattering is proposed[16], and in this study, fast terminal sliding mode control(FTSMC) using improved sliding faces is applied to ensure convergence within finite time[17–19].

Since it is difficult to ensure attitude stability through speed control only by the rotor of the multi-rotor due to disturbance, Control Moment Gyro (CMG), a driver device that generates torque using the Gyroscope effect, was applied to ensure attitude stability at a fast reaction speed[20–24]. CMG consists of flywheel and gimbal in structure, and can be classified into two main categories according to speed controllability of flywheel. VSCMG (Variable speed CMG) that adjusts the rotation speed of the wheel and the angle of the gimbal, and CSCMG (Constant speed CMG) that adjusts the angle of the gimbal[25, 26]. CMG has the advantage of being able to generate large torque with small inputs, and is mainly used for attitude control of high agility spacecrafts. Not limited to spacecrafts, related research is being conducted by applying it to various fields such as ships and vehicles, and recently, feasibility studies using CMG and reaction wheels as multi-rotor systems are being conducted[27–30]. Despite its excellent performance, CMG has a geometric singularity problem that cannot generate control torque in a specific direction.

This reason relates to the alignment of the CMG gimbal and the shape of the driver mounting, and the problem can be simplified according to the CMG mounting. The pyramid array structure, which is mainly used, is very difficult to avoid singularities due to the complexity of the singularity shape derived according to the tilt angle.

In this study, the CSCMG was used and two CMGs were attached side by side to the X-axis in the body frame. This form involves only roll and pitch movements, not yaw movements. The reason for using this form is that in the case of Yaw motion, the Z-axis moment of inertia of the multi-rotor is larger than that of other axes, and it is relatively less sensitive to disturbance. However, even in the case of the proposed form, it is not possible to have the same angular momentum distribution for all axes, and the maximum angular momentum allowed for each axis is closely related to the initial gimbal angle. If the multi-rotor fails to restore to the initial gimbal angle during hovering after starting, it is difficult to expect the same maneuver performance during all starts, and a singularity problem may occur. In order to overcome such singularity problems, research on various singularity avoidance and robust driving laws is continuously underway[20, 31–35]. In this study, we introduce the optimal angular momentum vector recovery driving law to prevent singularity problems. However, one further consideration in this driving law is the singularity problem due to disturbance. Therefore, we propose a Disturbance robust drive law, which can ensure the avoidance of singularities in CMGs by appropriately adjusting them to the torque by the rotor of the multi-rotor.

In this study, a hexa-rotor with higher thrust and more detailed control is used compared to a quad-rotor. To ensure flight stability and reliability, we apply FTSMC, which can guarantee robust and finite time convergence in disturbance and model uncertainty, and prove the stability of the control technique through Lyapunov theory. In addition, since it is difficult to guarantee attitude stability only by the rotor of the multi-rotor due to disturbance, two CSCMGs were applied, and DRSL was applied to solve the problem of CMG singularity. The designed system verifies the performance of CMG-free multirotors and CMG-free hexa-rotor through numerical simulations in the presence of disturbances.

II. Modeling of UAV

UAV is largely classified into fixed-wing method and rotary-wing method. The multi-rotor has the advantage of not being constrained by space because vertical VTOL and hoveing are possible through the thrust control of each rotor. Multi-rotors are classified into tri-rotors, quad-rotors, and hexa-rotors according to the number of rotors. In general, the most commonly used type of multi-rotor is a quad-rotor, which has the advantage of being relatively simple and intuitive in operation, but has the disadvantage of poor flight stability. In this study, a hexarotor that can withstand more power than a quadrotor and has excellent flight stability was used.

A. Coordinate System

In order to explain the dynamic motion of the hexarotor, two reference coordinate systems are required, and the coordinate systems are the inertial frame (X_E, Y_E, Z_E) and the body frame (X_B, Y_B, Z_B). The body frame of the hexarotor is a coordinate system fixed at the center of the actual observer or airplane, and the inertial frame is based on Newton's first law, so objects without force are stationary or move in a straight line at a constant speed. Basically, it is a coordinate system with the center of the Earth as the zero point. The structure of the hexarotor includes thrust, angular velocity, and torque by six rotors, and is shown as Fig.1[36–38]. The dynamic motion of the hexarotor can be explained by six degrees of freedom that appear in the 12 states of the hexarotor. Components expressed in the inertial frame are defined as position $\boldsymbol{\zeta}$, Euler angle $\boldsymbol{\eta}$ and Quaternion $\boldsymbol{Q}$. The Euler angle is intuitive, but there is a risk of loss of freedom due to the gimbal lock problem[39]. To overcome this problem, we use quaternion with no dependencies on other axes to solve the singularity problem and simplify the calculation. In this study, quaternion were used for mathematical modeling, and in order to intuitively interpret the operation of the hexarotor, it was analyzed by converting it into Euler angles. In the body

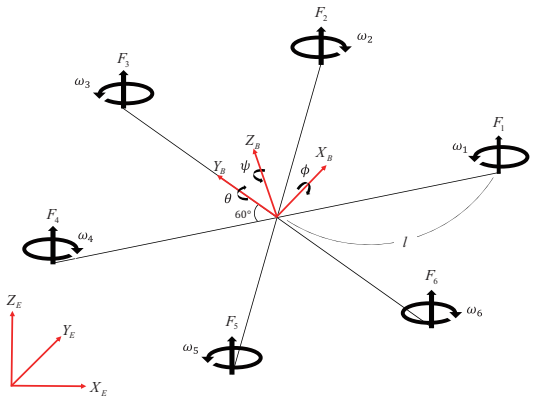

Figure. 1 Hexa-rotor configuration

frame, velocity is defined as $\boldsymbol{v}$, and angular velocity is defined as $\boldsymbol{\omega}$[40].

$$\boldsymbol{\xi}_E = \begin{bmatrix} X_E \\ Y_E \\ Z_E \end{bmatrix}, \quad \boldsymbol{\eta} = \begin{bmatrix} \phi \\ \theta \\ \psi \end{bmatrix} \& \boldsymbol{Q} = \begin{bmatrix} q_1 \\ q_2 \\ q_3 \\ q_4 \end{bmatrix} = \begin{bmatrix} \boldsymbol{q} \\ q_4 \end{bmatrix} \tag{1}$$

$$\boldsymbol{v} = \begin{bmatrix} v_x \\ v_y \\ v_z \end{bmatrix}, \quad \boldsymbol{\omega} = \begin{bmatrix} \omega_x \\ \omega_y \\ \omega_z \end{bmatrix} \tag{2}$$

B. Forece and Torque

The thrust of the rotor is represented by the lift coefficient and angular velocity of the rotor, and the thrust of the hexarotor is represented by the sum of the thrusts of the six rotors.

$$F_i = k\omega_i^2, \quad (i = 1, 2, 3, 4, 5, 6) \tag{3}$$

$$T = \sum_{i=1}^{6} F_i = k\sum_{i=1}^{6} \omega_i^2, \ \boldsymbol{T}_B = \begin{bmatrix} 0 \\ 0 \\ T \end{bmatrix} \tag{4}$$

where, k is the lift coefficient of the rotor, ω_i is angular speed of each rotor.

Hexarotor is rotated 60 degrees about the Z_B axis as shown in Fig.**??**, and Roll, Pitch, and Yaw moments can be obtained from the F_i and τ_i components of the body frame and geometric structure. At this time, the angular acceleration effect $\dot{\omega}_i$ of the rotor is small in the equation for the torque, so it is ignored.

$$\tau_i = b\omega_i^2 + \boldsymbol{J}_m\dot{\omega}_i \tag{5}$$

$$\tau_\phi = kl\left(\omega_3^2 - \omega_6^2 + \tfrac{1}{2}\left(-\omega_1^2 + \omega_2^2 + \omega_4^2 - \omega_5^2\right)\right)$$

$$\tau_\theta = kl\tfrac{\sqrt{3}}{2}\left(-\omega_1^2 - \omega_2^2 + \omega_4^2 + \omega_5^2\right) \tag{6}$$

$$\tau_\psi = b\left(-\omega_1^2 + \omega_2^2 - \omega_3^2 + \omega_4^2 - \omega_5^2 + \omega_6^2\right)$$

where, l is the distance from the center of the hexarotor to any of the propellers, b is the drag coefficient and $\boldsymbol{J}_m$ is the moment of inertia of the rotor.

Combining the thrust and torque equations, the equation for the control input of the hexarotor

can be obtained.

$$\begin{bmatrix} \tau_\phi \\ \tau_\theta \\ \tau_\psi \\ T_B \end{bmatrix} = \begin{bmatrix} u_1 \\ u_2 \\ u_3 \\ u_4 \end{bmatrix} = \mathbf{A}_{hexa} \begin{bmatrix} \omega_1^2 \\ \omega_2^2 \\ \omega_3^2 \\ \omega_4^2 \\ \omega_5^2 \\ \omega_6^2 \end{bmatrix}, \quad \boldsymbol{u} = \mathbf{A}_{hexa}\boldsymbol{X}_{hexa} \tag{7}$$

where, $\mathbf{A}_{hexa}$ is the motor driving matrix of the hexarotor.

$$\mathbf{A}_{hexa} = \begin{bmatrix} -\frac{kl}{2} & \frac{kl}{2} & kl & \frac{kl}{2} & -\frac{kl}{2} & -kl \\ -\frac{kl\sqrt{3}}{2} & -\frac{kl\sqrt{3}}{2} & 0 & \frac{kl\sqrt{3}}{2} & \frac{kl\sqrt{3}}{2} & 0 \\ -b & b & -b & b & -b & b \\ k & k & k & k & k & k \end{bmatrix} \tag{8}$$

C. Rotation Matrix

In order to derive the equation of motion of the hexarotor, it must be defined in one coordinate system. Quaternions are applied based on Euler's theory of rotation, which expresses the same variables as rotational motion in the translational motion of an arbitrary rigid body with fixed points. Quaternions, also known as Euler parameters, are defined as the main rotation factors as

$$\begin{aligned} q_1 &= p_1 \sin(\alpha/2) \\ q_2 &= p_2 \sin(\alpha/2) \\ q_3 &= p_3 \sin(\alpha/2) \\ q_0 &= \cos(\alpha/2) \end{aligned} \tag{9}$$

where, α is the angle of rotation with respect to the unit vector $\boldsymbol{p} = [p_1, p_2, p_3]$.

Please note that quaternions are composed of four elements, so there is a constraint that only one condition must be satisfied.

$$q_1^2 + q_2^2 + q_3^2 + q_0^2 = 1 \tag{10}$$

The direction cosine matrix from the body frame to the inertial frame is as follows.

$$\begin{aligned} \mathbf{R} &= \left(q_0^2 - \boldsymbol{q'q}\right)\mathbf{I}_{3\times 3} + 2\left(\boldsymbol{qq'}\right) + 2q_0\boldsymbol{q}^{\times} \\ &= \begin{bmatrix} q_0^2 + q_1^2 - q_2^2 - q_3^2 & 2\left(q_1q_2 - q_3q_0\right) & 2\left(q_2q_0 + q_1q_3\right) \\ 2\left(q_1q_2 + q_3q_0\right) & q_0^2 - q_1^2 + q_2^2 - q_3^2 & 2\left(q_2q_3 - q_1q_0\right) \\ 2\left(q_1q_3 - q_2q_0\right) & 2\left(q_1q_0 + q_2q_3\right) & q_0^2 - q_1^2 - q_2^2 + q_3^2 \end{bmatrix} \end{aligned} \tag{11}$$

where, $\mathbf{R}$ is orthogonal matrix; therefor, $\mathbf{R^{-1}} = \mathbf{R^T}$, $\boldsymbol{q}^{\times}$ is the matrix representation for the general vector product, which can be defined as a skew-symmetric matrix as follows.

$$\boldsymbol{q}^{\times} = \begin{bmatrix} 0 & -q_3 & q_2 \\ q_3 & 0 & -q_1 \\ -q_2 & q_1 & 0 \end{bmatrix} \tag{12}$$

D. Mathematical Model of the UAV

Through the rotation matrix, the relational expression between the velocity in the inertial frame and the velocity in the body frame can be expressed.

$$\begin{aligned}\begin{bmatrix}\dot{X}_E\\ \dot{Y}_E\\ \dot{Z}_E\end{bmatrix} &= \mathbf{R}\begin{bmatrix}v_x\\ v_y\\ v_z\end{bmatrix}\\ &= \begin{bmatrix}q_0^2+q_1^2-q_2^2-q_3^2 & 2(q_1q_2-q_3q_0) & 2(q_2q_0+q_1q_3)\\ 2(q_1q_2+q_3q_0) & q_0^2-q_1^2+q_2^2-q_3^2 & 2(q_2q_3-q_1q_0)\\ 2(q_1q_3-q_2q_0) & 2(q_1q_0+q_2q_3) & q_0^2-q_1^2-q_2^2+q_3^2\end{bmatrix}\begin{bmatrix}v_x\\ v_y\\ v_z\end{bmatrix}\end{aligned} \tag{13}$$

The kinematic differential equation for the quaternion is given by

$$\dot{\boldsymbol{Q}} = \frac{1}{2}\begin{bmatrix}0 & -\omega_x & -\omega_y & -\omega_z\\ -\omega_x & 0 & \omega_z & -\omega_y\\ \omega_y & -\omega_z & 0 & \omega_x\\ \omega_z & \omega_y & -\omega_x & 0\end{bmatrix}\begin{bmatrix}q_0\\ q_1\\ q_2\\ q_3\end{bmatrix} \tag{14}$$

or by transmutation, the kinematic differential equation can also be a another form written by

$$\dot{\boldsymbol{Q}} = \frac{1}{2}\begin{bmatrix}q_0 & -q_1 & -q_2 & -q_3\\ q_1 & q_0 & -q_0 & q_2\\ q_2 & q_3 & q_0 & -q_1\\ q_3 & -q_2 & q_1 & q_0\end{bmatrix}\begin{bmatrix}0\\ \omega_x\\ \omega_y\\ \omega_z\end{bmatrix} \tag{15}$$

The equation of motion for the attitude and position of the hexarotor can be described by the Newton-Euler equation. In the body frame, the centrifugal force $\boldsymbol{\omega}^{\times}(m\boldsymbol{v})$ and the force for mass acceleration $m\dot{\boldsymbol{v}}$ are equal to the gravitational force $\mathbf{R}^T\boldsymbol{G}$ and thrust $\boldsymbol{T}_B$ of the UAV. The acceleration in the body frame is as

$$m\dot{\boldsymbol{v}} + \boldsymbol{\omega}^{\times}(m\boldsymbol{v}) = \mathbf{R}^{\mathbf{T}}\boldsymbol{G} + \boldsymbol{T}_B \tag{16}$$

where, m is total mass of hexarotor, g is gravitational acceleration.

The expression for acceleration is as follows

$$\dot{\boldsymbol{v}} = \mathbf{R}^T \begin{bmatrix} 0 \\ 0 \\ g \end{bmatrix} - \boldsymbol{\omega}^{\times} \boldsymbol{v} + \frac{1}{m} \begin{bmatrix} 0 \\ 0 \\ T \end{bmatrix} \tag{17}$$

To enhance the actual behavior of the UAV, the aerodynamic effect created by air resistance must be included. Therefore, it can be expressed as

$$\dot{\boldsymbol{v}} = \mathbf{R}^T \begin{bmatrix} 0 \\ 0 \\ g \end{bmatrix} - \boldsymbol{\omega}^{\times} \boldsymbol{v} + \frac{1}{m} \begin{bmatrix} 0 \\ 0 \\ T \end{bmatrix} - \frac{1}{m} \begin{bmatrix} A_x & 0 & 0 \\ 0 & A_y & 0 \\ 0 & 0 & A_z \end{bmatrix} \begin{bmatrix} v_x \\ v_y \\ v_z \end{bmatrix} \tag{18}$$

In the body frame, the sum of the centripetal force $\boldsymbol{\omega}^{\times}\mathbf{J}_{hexa}\boldsymbol{\omega}$ and the inertial angular acceleration $\mathbf{J}_{hexa}\dot{\boldsymbol{\omega}}$ are equal to the torque $\boldsymbol{u}_{\eta}$. Application to rotational motion from Newton-Euler equation is as follows.

$$\mathbf{J}_{hexa}\dot{\boldsymbol{\omega}} = -\boldsymbol{\omega}^{\times}\mathbf{J}_{hexa}\boldsymbol{\omega} + \boldsymbol{u}_{\eta} \tag{19}$$

Adding disturbances here is as follows.

$$\dot{\boldsymbol{\omega}} = \mathbf{J}_{hexa}^{-1}\left(-\boldsymbol{\omega}^{\times}\mathbf{J}_{hexa}\boldsymbol{\omega} + \boldsymbol{u}_{\eta} + \boldsymbol{d}\right) \tag{20}$$

where,

$$\mathbf{J}_{hexa} = diag\begin{pmatrix} J_{hexa,xx} & J_{hexa,yy} & J_{hexa,zz} \end{pmatrix} \tag{21}$$

$$\boldsymbol{d} = \begin{bmatrix} \tau_{\phi,d} & \tau_{\theta,d} & \tau_{\psi,d} \end{bmatrix}^T \tag{22}$$

$$\boldsymbol{u}_{\eta} = \begin{bmatrix} \tau_{\phi} & \tau_{\theta} & \tau_{\psi} \end{bmatrix}^T \tag{23}$$

$J_{hexa,xx}, J_{hexa,yy}$ and $J_{hexa,zz}$ are the moments of inertia of the hexarotor in each axis direction, $\boldsymbol{d}$ is torque disturbance, $\boldsymbol{u}_{\eta}$ is torque of hexarotor.

III. Modeling of UAV Using CMGs

Currently, there is Control Moment Gyro (CMG), which is an actuator device that generates torque using flywheels among the attitude control devices of spacecrafts.In the case of the CMG, there is a difference in performance compared to the momentum wheel and the reaction wheel, which are other attitude control devices, and the performance part has torque that induces attitude control. In the case of the momentum wheel and the reaction wheel, the generation of torque is insufficient compared to the CMG, so there is a limit to the attitude control of the spacecrafts, which emphasizes maneuverability. In fact, in order to generate a large torque using a momentum wheel and a reaction wheel for attitude control of an object requiring high agility, the size of the wheel has to be increased, and strong motor performance is required accordingly. Therefore, weight and power consumption increase inefficiently. However, if the CMG is used, since the torque is amplified by the principle of the gyroscopic effect, it is possible to generate a larger torque for the same size wheel and motor performance. CMG has a unique advantage of torque amplification, and research is being actively conducted to compensate for the problems of expensive equipment, complexity, and singularity. In this study, the validity of the multi-rotor attitude control is confirmed using the characteristics of CMG.

A. System Configuration

As shown in Fig.2, it is defined as a gimbal frame given by unit vectors (a, b, c) and body frame. a is the unit vector of the gimbal axis. b is the unit vector of the spinning axis of the wheel disk. c is the unit vector of the torque axis. Components of the gimbal frame unit vector are assumed to be given by the hexarotor body reference frame. The structure of CMG is composed of gimbal rotor, spin rotor, and flywheel, and can be classified into two main categories according to speed controllability of flywheel. It is classified into Variable speed CMG (VSCMG), which controls the rotational speed of the wheel and the angle of the gimbal, and Constant speed CMG (CSCMG), which maintains a constant rotational speed of the wheel and adjusts the angle of the gimbal. It is classified according to the number of gimbal axes, and if there is one, it is divided into single gimbal CMG and double gimbal CMG if there are two. In this study, attitude control was performed using two CSCMGs.

In this study, as shown in Fig.3, in order to solve the singularity problem relatively simply, the CSCMG method was applied to select a method of attaching two CMGs side by side to the X-axis of the body frame. This form is involved in roll and pitch motions, but not in yaw motion. The reason for choosing this form is that in the case of yaw motion, the Z-axis moment of inertia of the hexarotor is larger than that of other axes, so it is relatively less sensitive to disturbance. Therefore, a form that can only be involved in roll and pitch motions was selected.

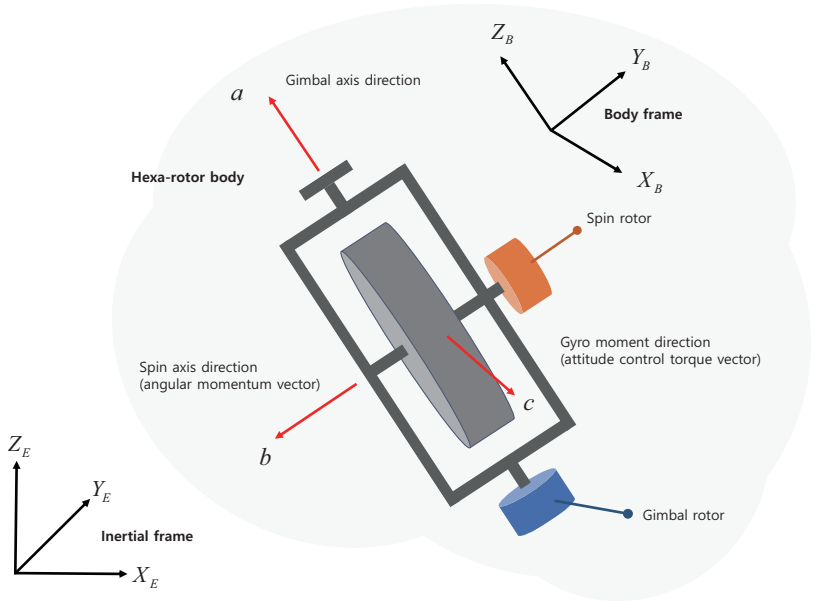

Figure. 2 Rigid hexa-rotor body with a single CMG

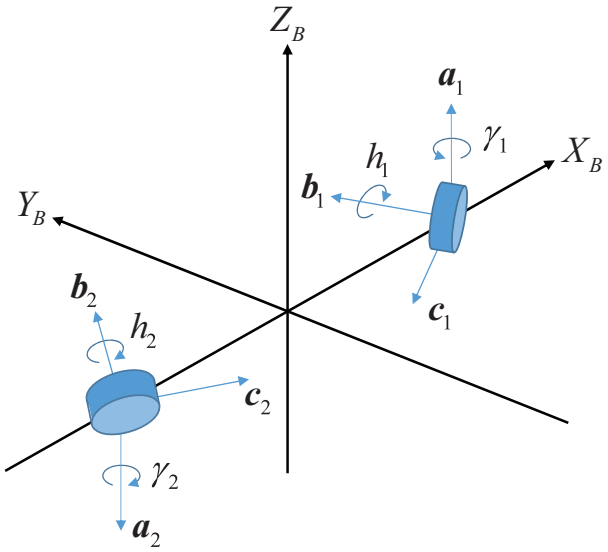

Figure. 3 Definition of Two CSCMGs Coordinate System

B. Mathematical Model of the UAV with CMGs

The CMG attached to the hexarotor can be expressed in the body frame of the hexarotor and the gimbal frame of the CMG, and the rotation matrix for converting the gimbal frame to the body frame is defined as $\mathbf{C}$.

$$\mathbf{C} = \begin{bmatrix} \boldsymbol{a} & \boldsymbol{b} & \boldsymbol{c} \end{bmatrix} \tag{24}$$

From the CSCMG, the derivatives of the unit vectors are given by

$$\begin{aligned} \dot{a}_i &= 0 \\ \dot{b}_i &= \dot{\gamma}_i c_i \\ \dot{c}_i &= -\dot{\gamma}_i b_i \end{aligned} \tag{25}$$

Consider a hexarotor applied with two CSCMGs rotating with the angular velocity $\boldsymbol{\omega}$ of the hexarotor body, the spin rate ω_w of the wheel disk with respect to the gimbal frame and gimbal rate $\dot{\gamma}$ of the gimbal frame with respect to the body frame.

$$\begin{aligned} \dot{\boldsymbol{\gamma}}_g &= \begin{bmatrix} \dot{\gamma} & 0 & 0 \end{bmatrix}^T \\ \dot{\boldsymbol{\omega}}_w &= \begin{bmatrix} 0 & \omega_w & 0 \end{bmatrix}^T \end{aligned} \tag{26}$$

The angular velocity of the hexarotor relative to the body frame can be converted to the gimbal frame as follows.

$$\begin{aligned} \boldsymbol{\omega} &= \omega_x \boldsymbol{x} + \omega_y \boldsymbol{y} + \omega_z \boldsymbol{z} \\ &= \omega_a \boldsymbol{a} + \omega_b \boldsymbol{b} + \omega_c \boldsymbol{c} = \mathbf{C}\boldsymbol{\omega}_g \end{aligned} \tag{27}$$

where $\boldsymbol{\omega}_g$ is angular vector with respect to the gimbal frame. The projection of the angular vector onto the gimbal frame has a relationship given by

$$\boldsymbol{\omega} = \mathbf{C}\boldsymbol{\omega}_g \tag{28}$$

The gimbal direction unit vector $\boldsymbol{a}$ is an axis fixed to the body frame, and when the gimbal angle γ is rotated around this axis, the gimbal angular velocity appears. The gimbal angular

velocity vector is

$$\dot{\boldsymbol{\gamma}}_g = \dot{\gamma}\boldsymbol{a} = \begin{bmatrix} \dot{\gamma} & 0 & 0 \end{bmatrix}^T \tag{29}$$

The total angular momentum of the CSCMG can be expressed as

$$\boldsymbol{h}_{cmg} = \sum_{i=1}^{2} h_i b_i \tag{30}$$

where $\boldsymbol{h}_{cmg}$ is the angular momentum vector of CSCMG, $h_i = J_i \omega_{\omega,i}$ represents the i-th internal momentum produced by the i-th CSCMG, and J_i denotes the moment of inertia of the i-th CSCMG wheel.

The time derivative of $\boldsymbol{h}_{cmg}$ is equal to the torque generated by the CSCMGs as follows.

$$\begin{aligned} \dot{\boldsymbol{h}}_{cmg} &= \sum_{i=1}^{2} \dot{h}_i b_i + \sum_{i=1}^{2} h_i \dot{b}_i \\ &= \sum_{i=1}^{2} J_i \dot{\omega}_{\omega,i} b_i + \sum_{i=1}^{2} h_i \dot{\gamma}_i c_i = \mathbf{u}_{cmg} \end{aligned} \tag{31}$$

where $\boldsymbol{u}_{cmg}$ represents the torque output vector. Since CSCMG was selected in this study, the angular velocity ω_ω is set to 0. Therefore, it can be written as

$$\begin{aligned} \boldsymbol{u}_{cmg} &= \sum_{i=1}^{2} h_i \dot{\gamma}_i c_i \\ &= \begin{bmatrix} h_1 c_1 & h_2 c_2 \end{bmatrix} \begin{bmatrix} \dot{\gamma}_1 \\ \dot{\gamma}_2 \end{bmatrix} \\ &= \mathbf{A}(\gamma)\dot{\boldsymbol{\gamma}} \end{aligned} \tag{32}$$

$$\mathbf{A}(\gamma) = \begin{bmatrix} -h_1 \cos\gamma_1 & h_2 \cos\gamma_2 \\ -h_1 \sin\gamma_1 & -h_2 \sin\gamma_2 \\ 0 & 0 \end{bmatrix} \tag{33}$$

where A is the jacobian matrix. The detailed derivation of the equations of motion without simplification is well described in Refs.[26, 33, 41].

To derive the equation of motion of a hexarotor with two CSCMGs installed, the total angular

momentum vector $\boldsymbol{h}$ of a hexarotor with CMGs is as follows.

$$\boldsymbol{h} = \boldsymbol{h}_{hexa} + \boldsymbol{h}_{cmg} \tag{34}$$

where, $\boldsymbol{h}_{hexa}$ is the angular momentum vector of the hexarotor, and $\boldsymbol{h}_{cmg}$ is the angular momentum vector of the two CSCMGs.

Equations of motion of the system from Euler's equation is given by

$$\dot{\boldsymbol{h}} = \boldsymbol{u} \tag{35}$$

In order to derive the time change of the total angular momentum vector $\boldsymbol{h}$ of the hexarotor, the components of Eq.34 are differentiated with respect to each time, and summarized as follows.

$$\mathbf{J}\dot{\boldsymbol{\omega}} = -\boldsymbol{\omega}^{\times}\mathbf{J}\boldsymbol{\omega} + \boldsymbol{\omega}^{\times}\boldsymbol{h}_{cmg} - \mathbf{A}\left(\gamma\right)\dot{\boldsymbol{\gamma}} + \boldsymbol{u}_{\eta} + \boldsymbol{d} \tag{36}$$

where, $\mathbf{J}$ is the total moment of inertia of the hexarotor including the two CSCMGs, $\boldsymbol{\omega}$ is the angular velocity vector of the hexarotor, $\boldsymbol{\omega}^{\times}$ is the skew-symmetric matrix for the angular velocity vector, and $\boldsymbol{d}$ is the disturbance.

and

$$\begin{aligned}
\mathbf{J} &= diag\begin{pmatrix} J_{xx} & J_{yy} & J_{zz} \end{pmatrix} \\
\boldsymbol{\omega} &= \begin{bmatrix} \omega_x & \omega_y & \omega_z \end{bmatrix}^T \\
\boldsymbol{\omega}^{\times} &= \begin{bmatrix} 0 & -\omega_3 & \omega_2 \\ \omega_3 & 0 & -\omega_1 \\ -\omega_2 & \omega_1 & 0 \end{bmatrix} \\
\dot{\boldsymbol{\gamma}} &= \begin{bmatrix} \dot{\gamma}_1 & \dot{\gamma}_2 \end{bmatrix}^T \\
\boldsymbol{d} &= \begin{bmatrix} \tau_{\phi,d} & \tau_{\theta,d} & \tau_{\psi,d} \end{bmatrix}^T
\end{aligned} \tag{37}$$

IV. Sliding Mode Control

Most control techniques have limitations in modeling nonlinear dynamics and handling various environmental variables, and it is expected that it will be difficult to respond accurately and promptly to work under disturbance and model uncertainty. Sliding mode control(SMC), which follows the target state accurately and quickly and is robust to disturbance and model uncertainty, can handle nonlinear dynamics without linearization, define a sliding surface using system state variables, and control variables to make the system behave[42]. SMC is controlled through two operations. The first step is the reaching phase of the variable to be controlled toward the sliding surface. The second is the sliding phase, in which the variable that rises above the surface flows toward the target value. Generally, the variable you want to control is defined as the error between the current state and the target state. Designed the controller to aim to zero error.

The typical sliding mode control has the disadvantage that it takes infinite time for the state error to converge to zero. To compensate for this, Terminal Sliding Mode Control(TSMC) was proposed, and in this control method, Fast Terminal Sliding Mode Control(FTSMC) was proposed to allow the error to converge to zero more quickly. In this study, FTSMC was used for attitude control and TSMC was used for altitude control.

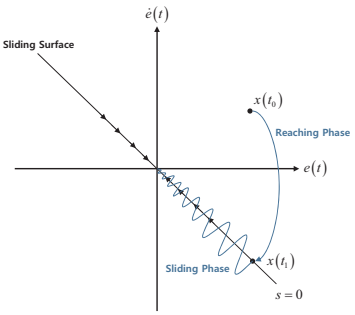

Figure. 4 Phase Portrait of Sliding Mode Control

A. Altitude Control

The Terminal Sliding Mode Control (TSMC) technique is one of the control methods that solves the disadvantage that it takes infinite time for each variable to converge to 0. By applying this technique, convergence to the target value can be guaranteed within a finite time. For altitude control, TSMC was applied. The sliding surface and error equation for this are defined as follows.

$$s_z = \dot{e} + a_z e^{r_z} \tag{38}$$

$$e_z = z - z_d. \tag{39}$$

where, a_z is positive gain values greater than zero, and r_z is gain values having a value between 0 and 1.

To obtain the convergence time of TSMC, we assume that the sliding surface is

$$s_z = \dot{e} + a_z e^{r_z} = 0 \tag{40}$$

thus,

$$\dot{e} = -a_z e^{r_z} \tag{41}$$

The above equation can be viewed as a first-order differential equation for time, and integration is performed to obtain the convergence time.

$$\int_{e_s}^{e_f} e^{-r_z} de = -a_z \int_{t_s}^{t_f} dt \tag{42}$$

where, e_s and e_f mean the initial error and final error, and t_s and t_f mean the start time and final time.

Integration by parts, and assuming that the final error ef and the starting time ts are zero,

$$\left[\frac{1}{1-r_z} e^{1-r_z}\right]_{e_s}^{e_f} = -a_z \left[t\right]_{t_s}^{t_f} \tag{43}$$

$$\frac{1}{1-r_z} e^{1-r_z} = -a_z t_f \tag{44}$$

By rearranging the final time ts, the convergence time of TSMC can be obtained, and convergence of each variable within a finite time can be guaranteed.

$$t_f = \frac{1}{a_z\left(1-r_z\right)} e_s^{1-r_z} \tag{45}$$

In order to obtain the control input for the altitude control of the hexarotor, it can be obtained by differentiating the equation for the sliding surface of Eq.38 with respect to time and rearranging for u_z.

In this study, the power rate reaching law is selected as the reaching law consisting of the sum of the proportional terms for the sliding surface. This type of reaching law is used in many studies because it not only reduces chattering but also has good control performance.

$$\dot{s}_z = -\lambda_{z1} s_z - \lambda_{z2} |s_z|^{p_z} sign\left(s_z\right) \tag{46}$$

where, $\lambda_{z,1}$ and $\lambda_{z,2}$ are positive gain values greater than zero, and p_z is gain values having a value between 0 and 1.

The sliding surface of Eq.38 has a problem that an imaginary number appears when the state variable e is negative. To solve this, we use a modified sliding surface as follows.

$$s_z = \dot{e} + a_z |e|^{r_z} sign\left(e\right) \tag{47}$$

where, sign $(\cdot)$ are signum functions.

Using the modified sliding surface, the control input for the altitude control of the hexarotor can be derived as follows.

$$u_4 = \frac{m}{R_z}\left(-a_z r_z |e|^{r_z - 1}\dot{e} + g + \dot{s}_z\right) \tag{48}$$

where, R_z are values corresponding to 3 rows and 3 columns in eq.11.

Lyapunov function is used to verify the stability of the system using the designed controller. The goal of the controller is to make the sliding variable zero, and the Lyapunov candidate function is defined as follows.

$$V = \frac{1}{2} s_z^2 \tag{49}$$

Differentiating the Lyapunov candidate function gives

$$\dot{V} = s_z \dot{s}_z = s_z \left(-\lambda_{z1} s_z - \lambda_{z2} |s_z|^{p_z} sign\left(s_z\right) \right) < 0 \tag{50}$$

Therefore, since it can be seen that it is less than 0, the controller is Lyapunov stable, and the sliding surface converges to 0 after sufficient time.

B. Attitude Control

Fast Terminal Sliding Mode Control (FTSMC) is a control technique that speeds up the convergence speed in the existing TSMC. The sliding surface of FTSMC is as follows.

$$\boldsymbol{s} = \dot{\boldsymbol{e}} + a_\eta \boldsymbol{e} + b_\eta \dot{\boldsymbol{e}}^r \tag{51}$$

where, a_η and b_η are positive gain values greater than zero, and r is gain values having a value between 0 and 1.

FTSMC ensures a faster convergence rate compared to TSMC. The method of calculating the convergence speed is the same as that of TSMC. It is guaranteed that each variable converges to 0 within time $t = ln((a_\eta e_s^{1-r} + b_\eta)/b_\eta)/(a_\eta(1-r))$. The sliding surface, like the sliding surface of TSMC, has the problem of appearing imaginary numbers when the variable is negative. The problem was solved in the same way as TSMC, and for attitude control, the error equation is defined using the desired quaternion $\boldsymbol{q}_d$ and the sliding surface in which the sliding variable is 0 is as follows.

$$\boldsymbol{s}_\eta = \left[s_\phi, s_\theta, s_\psi\right]^T = \boldsymbol{\omega} + a_\eta \mathbf{Q}_e + b_\eta G(\mathbf{Q}_e)^r \mathrm{sgn}\left(\mathbf{Q}_e\right) \tag{52}$$

$$\mathbf{Q}_e = \begin{bmatrix} \boldsymbol{q}_e \\ q_{e,4} \end{bmatrix} = \begin{bmatrix} q_{d,4}\mathbf{I_{3\times 3}} - \boldsymbol{q}_d^\times & -\boldsymbol{q}_d \\ \boldsymbol{q}_d^T & q_{d,4} \end{bmatrix} \begin{bmatrix} \boldsymbol{q} \\ q_0 \end{bmatrix} \tag{53}$$

In order to obtain a control input for attitude control of the hexarotor, the equation for the sliding variable is differentiated with respect to time as follows.

$$\dot{\boldsymbol{s}}_\eta = -\lambda_1 \boldsymbol{s}_\eta - \lambda_2 G(\boldsymbol{s}_\eta)^p \mathrm{sgn}\left(\boldsymbol{s}_\eta\right) \tag{54}$$

where, sign $(\cdot)$ are signum functions, λ_1, $\lambda_2$are positive gain values greater than zero, p is gain values having a value between 0 and 1.

Using the above equations, the control input for the attitude of the hexarotor can be obtained as follows.

$$\boldsymbol{u}_\eta = \boldsymbol{\omega}^\times \mathbf{J}\omega - \mathbf{J}\left(-\dot{\boldsymbol{s}} + \left(a_\eta \mathbf{I}_{3\times 3} + b_\eta r G(\boldsymbol{Q}_e)^{r-1}\right)\frac{1}{2}\left(\boldsymbol{Q}_e^\times + q_0 I_3\right)\boldsymbol{\omega}\right). \tag{55}$$

where,

$$G\left(\boldsymbol{s}\right) = diag\left(\left|s_{\phi}\right|, \left|s_{\theta}\right|, \left|s_{\psi}\right|\right) \tag{56}$$

$$\mathrm{sgn}\left(q_i\right) = \left[sign\left(q_1\right), sign\left(q_2\right), sign\left(q_3\right)\right]^T \tag{57}$$

Lyapunov theory is used to verify the stability of the system using the designed controller. At this time, in order to verify the robustness of FTSMC, it is confirmed through the modeling equation Eq.20 considering the disturbance. The goal of the controller is to make the sliding variable zero, and the Lyapunov candidate function is defined as follows.

$$V = \frac{1}{2}\boldsymbol{s}_{\eta}^{T}\mathbf{J}\boldsymbol{s}_{\eta} \tag{58}$$

Differentiating the Lyapunov candidate function gives

$$\dot{V} = \boldsymbol{s}_{\eta}^{T}\mathbf{J}\dot{s}_{\eta} = \boldsymbol{s}_{\eta}{}^{T}\left(-\lambda_1\boldsymbol{s}_{\eta} - \lambda_2 G(\boldsymbol{s}_{\eta})^{p} sgn\left(\boldsymbol{s}_{\eta}\right)\right) < 0 \tag{59}$$

Therefore, since it can be seen that it is less than 0, the controller is Lyapunov stable, and the sliding surface converges to 0 after sufficient time.

C. Numerical Simulation

1. Simulation Configuration

Using the sliding mode control, a control performance comparison simulation of a hexarotor with and without two CSCMGs is conducted. In addition, the performance was compared and analyzed in an environment without disturbance and in an environment with disturbance. For accurate performance comparison, Since the hexarotor control the attitude through the thrust control of six motors, a mathematical model for the motor must also be considered. Therefore, the simple mathematical model of the BLDC motor used in the hexarotor is as follows.

$$\dot{\omega}_m = \frac{K_m}{J_m R_m}\left(-K_b \omega_m + V\right) \tag{60}$$

where, w_m is the motor angular velocity, J_m is the moment of inertia of the motor, K_m is the torque constant, R_m is the motor resistance, K_b is the back electromotive force and V is the voltage.

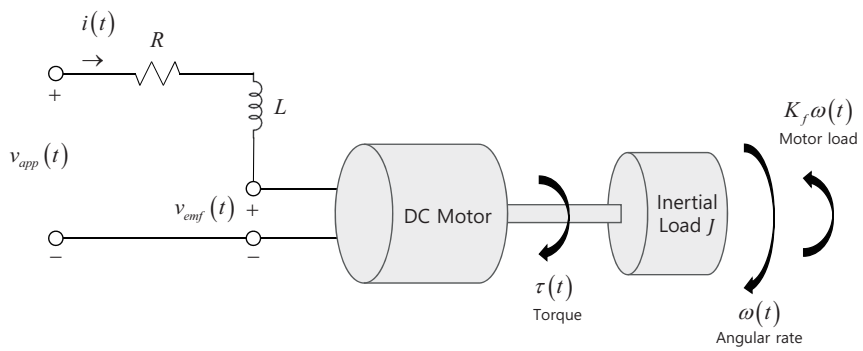

Figure. 5 A Simple Model of a DC Motor Driving

The hexarotor system parameters and SMC gains used in the simulation are shown in Table.1 and 2, respectively. The initial attitude of the hexarotor was set as $\eta_0 = [0,0,0]^T deg$, and the target attitude was set as $\eta_d = [10,20,30]^T deg$. The altitude was simulated with the goal of maintaining $5m$.

The disturbance scenario was designed with a torque value as shown in Fig.6, and the simulation was conducted by adding the torque value to the hexarotor modeling formula.

Table 1: Configuration of hexarotor with CSCMGs system

Variable	**Parameter**	**Variable**	**Parameter**
η_0 (deg)	$[0,0,0]^T$	η_d (deg)	$\begin{bmatrix}0\\0\\0\end{bmatrix} \rightarrow \begin{bmatrix}10\\20\\30\end{bmatrix} \rightarrow \begin{bmatrix}0\\0\\0\end{bmatrix}$
$z_0\,(m)$	5	$z_d\,(m)$	5
$J_{xx}\,(kgm^2)$	0.17	$m\,(kg)$	6.7
$J_{yy}\,(kgm^2)$	0.175	$l\,(m)$	0.96
$J_{zz}\,(kgm^2)$	0.263	b	0.001
k	0.03	$h_i\,(Nms)$	0.2
$\gamma_0\,(deg)$	45	$J_m\,(kgm^2)$	9.68×10^{-6}
$K_b\,(V/krpm)$	6.3×10^{-3}	$R_m\,(\Omega)$	3
$K_m\,(Nm/A)$	6.3×10^{-3}		

Table 2: Design parameters for SMC

Parameter	**Values**	**Parameter**	**Values**
a	0.5	b	0.5
λ_1	12	λ_2	9
r	0.95	p	0.95

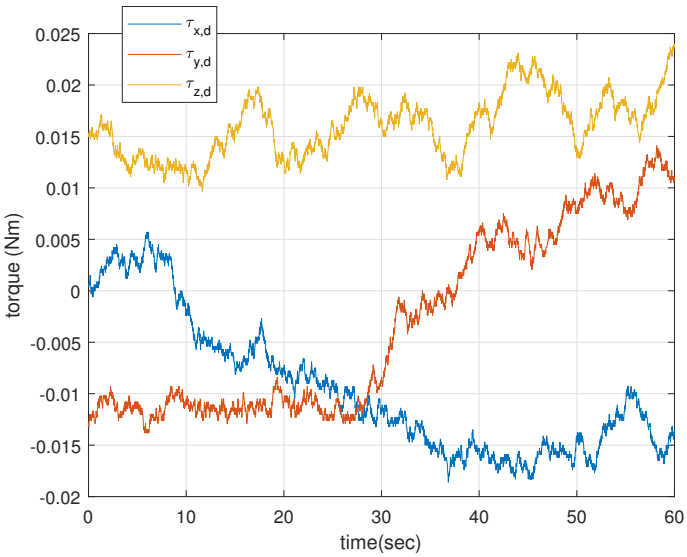

Figure. 6 Disturbance scenario

2. Without CMG Simulation Result

A simulation is conducted to control the attitude of a hexarotor without CMG in an environment without and with disturbance. Figure.7 and 8 are the attitude and attitude error graphs of the hexarotor. When there is no disturbance, as shown in the results of Fig.7(a) and Figure.8(a), it can be confirmed that the attitude value converges to the target attitude even though there is a slight tremor. In the case of disturbance, the attitude value fluctuated as shown in Fig.7(b) and Fig.8(b). In the case of the pitch, there was a maximum error of -0.27 deg due to disturbance of about -0.01 Nm in the range of 0 to 20 seconds. In the case of roll, there was a maximum error of -0.47 deg due to disturbance of about -0.01 Nm in the 20 to 40 second section. Figure.9 and 10 are the motor speed and torque graphs of the hexarotor. It can be seen that the tremor phenomenon appears both in the absence of disturbance and in the presence of disturbance. This phenomenon is caused by the sign function in the arrival law and is called chattering. During hovering and attitude conversion, when controlled only by the motor in an environment with disturbance, it can be seen that a lot of vibration occurs as the motor does not respond quickly enough to compensate for the disturbance.

FTSMC can be controlled to converge faster by adjusting the gain, but it has a problem of poor compensating ability for disturbance. Conversely, when the disturbance capability increases, there is a problem that the convergence speed becomes slow, and it is necessary to tune an appropriate gain more suitable for the control purpose among disturbance and control performance. It can be seen that vibration occurs even when there is no disturbance due to the strong gain tuning against disturbance. And, it was confirmed that it is difficult to compensate for the disturbance only with the motor of the hexarotor in an environment with disturbance.

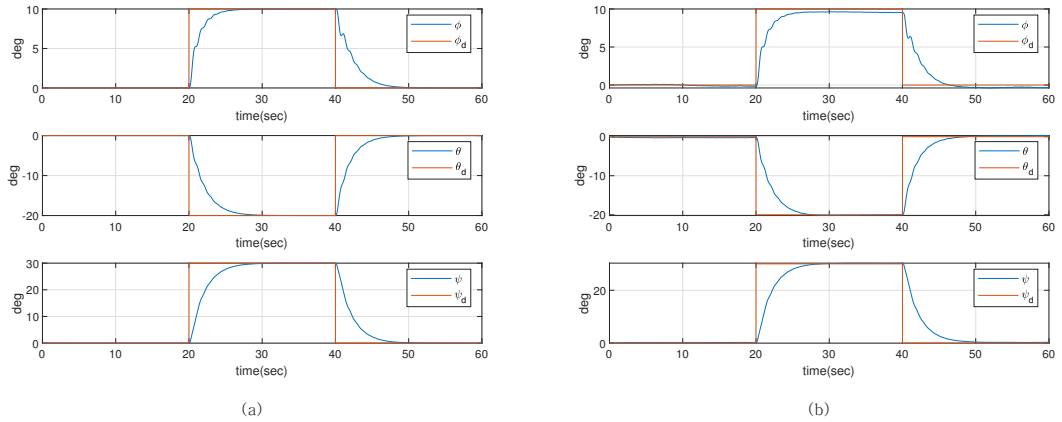

(a) (b)

Figure. 7 Histories of Attitude Without CMGs (a) without disturbance, (b) with disturbance

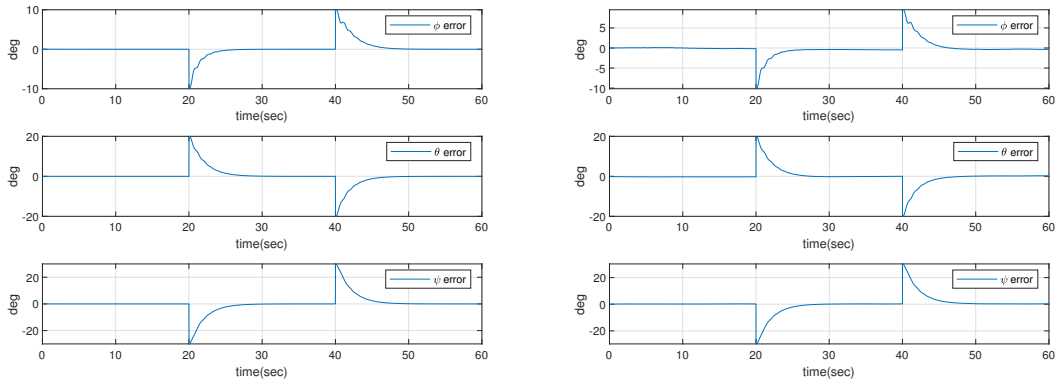

(a) (b)

Figure. 8 Histories of Attitude Error Without CMGs (a) without disturbance, (b) with disturbance

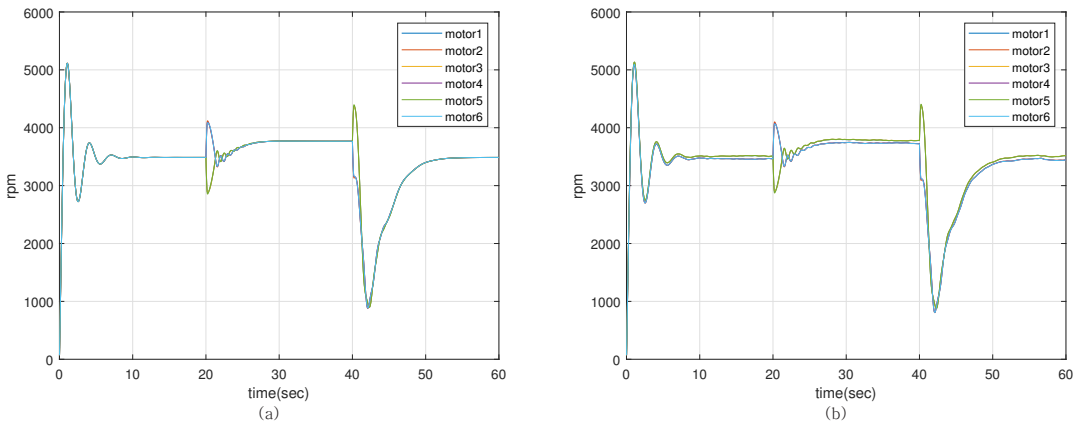

Figure. 9 Histories of Motor Speed Without CMGs (a) without disturbance, (b) with disturbance

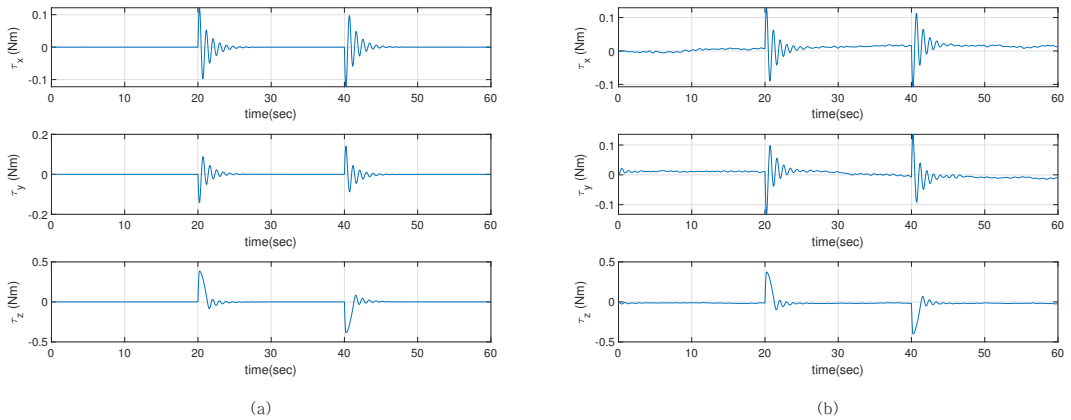

Figure. 10 Histories of Torque Without CMGs (a) without disturbance, (b) with disturbance

3. With CMG Simulation Result

A simulation is conducted to control the attitude of a hexarotor with CMG in an environment without and with disturbance. Figure.11 and 12 are the attitude and attitude error graphs of the hexarotor. When there is no disturbance, it can be confirmed that all converge to the target attitude as shown in the results of Fig.11(a) and Fig.12(a). In the case of disturbance, as shown in Fig.11(b) and Fig.12(b), in the case of the pitch, there is a maximum error of -0.15 deg due to the disturbance of about -0.01 Nm in the range of 0 to 20 seconds. In the case of roll, there is a maximum error of -0.16 deg due to disturbance of about -0.01 Nm in the range of 20 to 40 seconds. In the case of yaw, the performance of yaw does not change because only roll and pitch are involved due to the geometrical reason of CMG. However, it can be confirmed that all of them converge to the target attitude. Figure.13 and 14 are hexarotor motor speed and torque graphs. In the case of the speed of the motor, it can be seen that the vibration phenomenon appears at about 20 seconds both when there is no disturbance and when there is disturbance. This phenomenon is caused by the sign function in the arrival law and is called chattering. When there is no disturbance, the torque value of the hexarotor trembles when changing attitude. The reason is that vibration occurs even when there is no disturbance due to the strong gain tuning of the FTSMC gain adjustment against disturbance. Figure.15 is the angle graph of the CMG gimbal. The initial gimbal angle γ_0 was set to 45 deg. It converged to the initially set gimbal angle while entering the hovering state with the final attitude command value in an environment without disturbance, and γ_1 had a 5 deg error. It was confirmed that the final hovering did not converge to the initial gimbal angle in an environment with disturbance. Figure.16 is the angular velocity graph of the CMG gimbal. In the absence of disturbance, the maximum angular velocities of $\dot{\gamma}_1$ and $\dot{\gamma}_2$ are about 2 rad/s and 4 rad/s, respectively, and in the presence of disturbance, the maximum angular velocities of $\dot{\gamma}_1$ and $\dot{\gamma}_2$ are about 0.6 rad/s and 5.5 rad/s, respectively.

Therefore, it was confirmed that stability and convergence were improved when controlled using CMG compared to when controlling the attitude of the hexa-rotor only with the motor in an environment with disturbance. However, the initial gimbal angular position is closely related to the rotational maneuvering performance of the hexarotor. Because the angular momentum vectors for all axes are a function of the gimbal angle, they always change with changes in the

CMG gimbal vectors. One of the most important parts is that the same starting performance must be exhibited within all starting times. That is, the gimbal angle must always return to the initially defined direction. If you don't return, you will fall into the Singularity. As shown in Figure.11(b), in the case of roll, it can be seen that the error gradually increases at the end of the flight. Therefore, an angular momentum vector recovery drive law is required to recover the angular momentum vector.

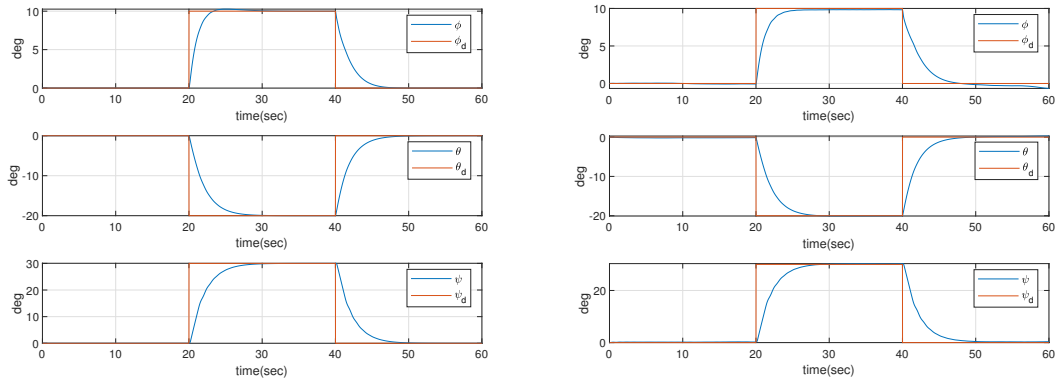

(a) (b)

Figure. 11 Histories of Attitude with CMGs (a) without disturbance, (b) with disturbance

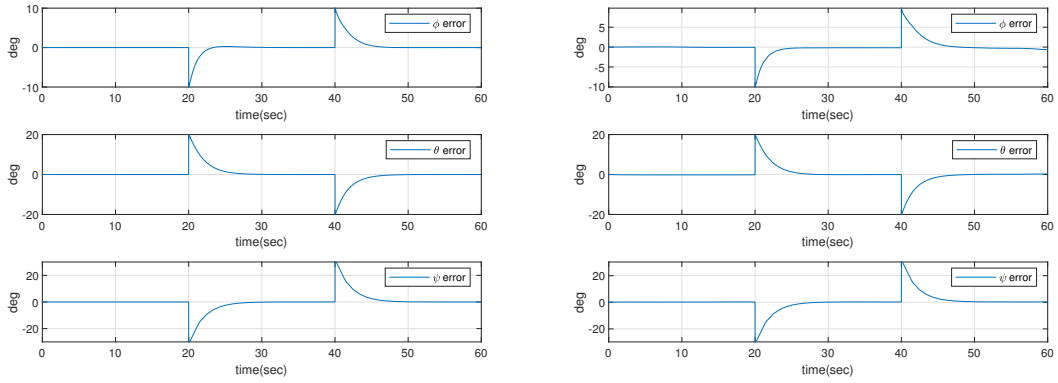

(a) (b)

Figure. 12 Histories of Attitude Error with CMGs (a) without disturbance, (b) with disturbance

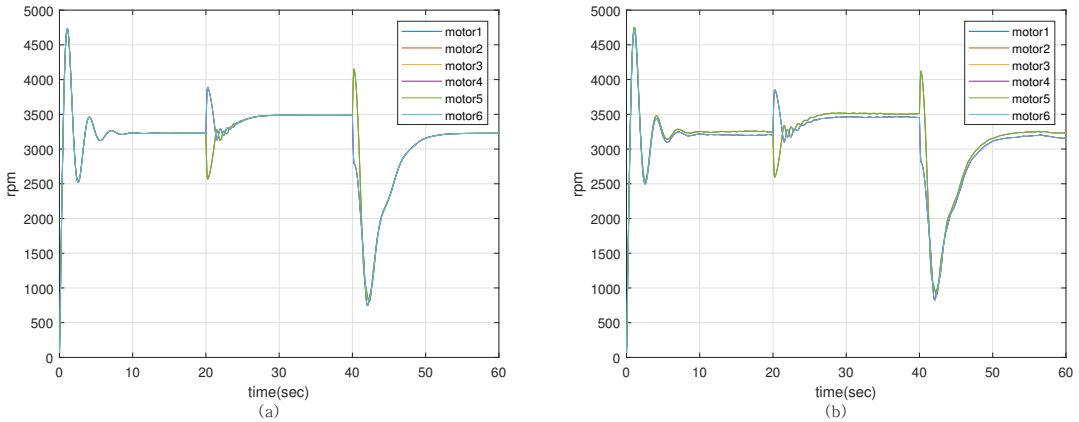

Figure. 13 Histories of Motor Speed with CMGs (a) without disturbance, (b) with disturbance

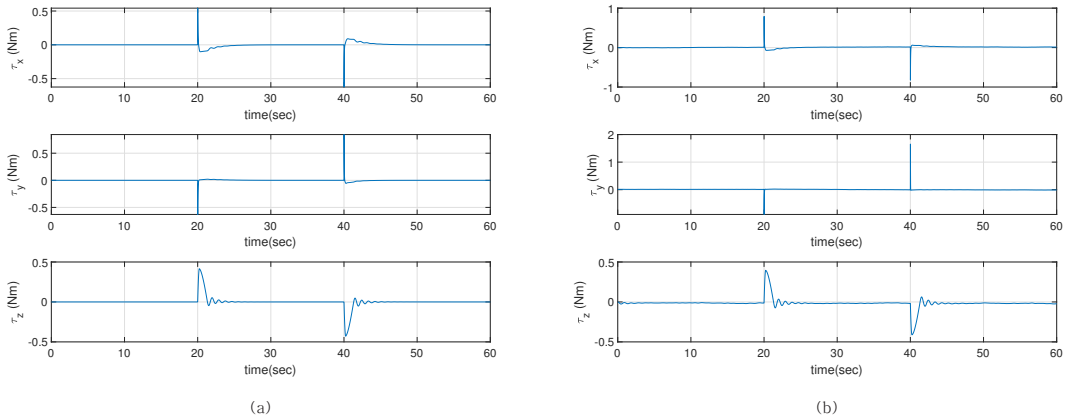

Figure. 14 Histories of Torque with CMGs (a) without disturbance, (b) with disturbance

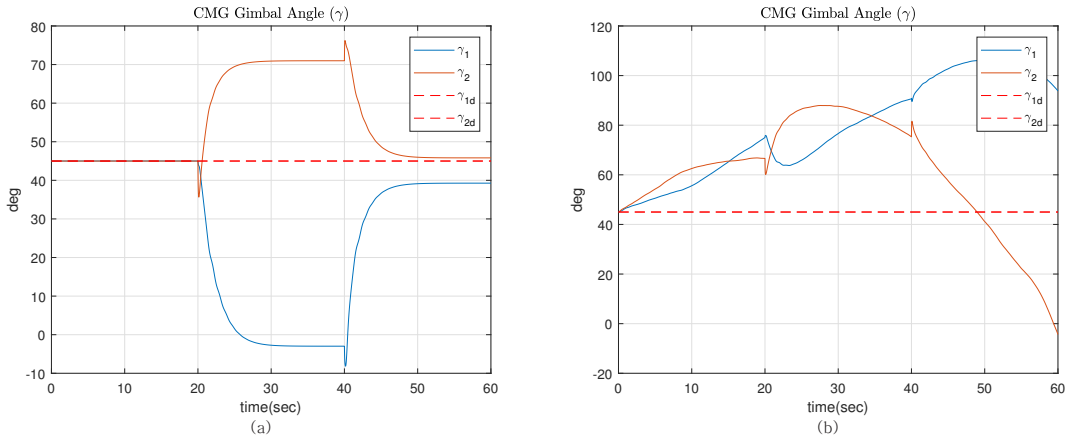

Figure. 15 Histories of Gimbal Angle with CMGs (a) without disturbance, (b) with disturbance

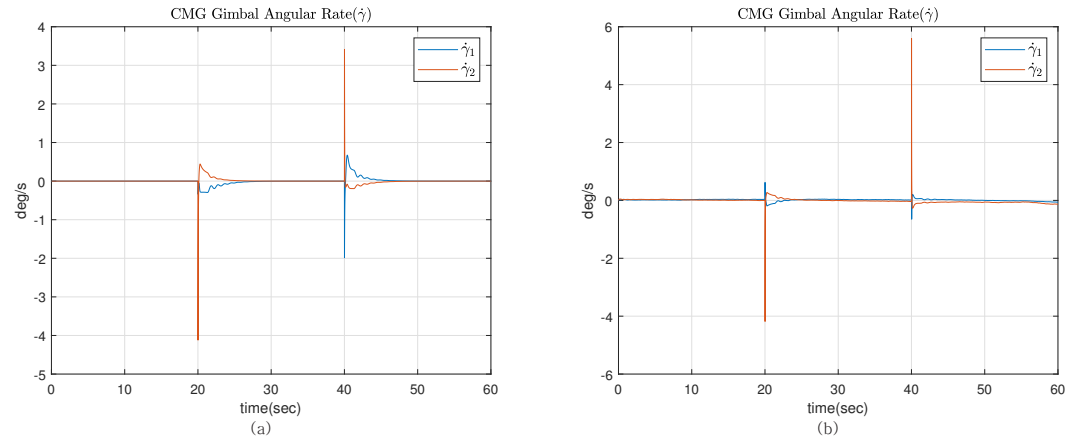

Figure. 16 Histories of Gimbal Rate with CMGs (a) without disturbance, (b) with disturbance

V. CMG Drive Law

The actuator command distribution law is required to generate the 3-axis control torque command derived from the attitude control law for the hexarotor attitude. At this time, control torque distribution is generally performed using Psudo-inverse drive law. In addition, when the torque command to be provided by the CMG is $\boldsymbol{u}_{cmg} = \dot{\boldsymbol{h}}$, it is equal to the product of the jacobian matrix $\mathbf{A}(\gamma)$ and angular velocity of the gimbal, and the inverse of the jacobian matrix is required to obtain the angular velocity of the gimbal $\dot{\gamma}$ required to drive the CMG from the torque. However, since the jacobian matrix is not a square matrix, the angular velocity value is obtained using the psudo-inverse matrix. However, since the Jacobian matrix of the pseudo-inverse matrix law is also a function of the gimbal angle, the pseudo-inverse matrix for the CMG of a specific gimbal angle configuration does not always exist. The singular state occurs when the rank value of the jacobian matrix is less than 3. Consequently, the gimbal angular velocity cannot be calculated. Therefore, there are various studies on the CMG drive law to avoid and escape from the following singular state.

The initial gimbal angular position is closely related to the rotational maneuvering performance of the hexarotor. Because the angular momentum vectors for all axes are a function of the gimbal angle, the values always change with changes in the CMG gimbal vectors. If it is one of the most important parts that the same maneuvering performance must be demonstrated within all maneuvering times, the angular momentum vector allowed for each axis must not change its value before starting the attitude maneuver. This means that the gimbal angle should always return to the initial gimbal angle. As a result, the angular momentum vector must also return to the initial angular momentum vector position at the time of the last posture maneuver of any hexarotor. If it fails to return and gradually moves away from the value of the initial angular momentum vector, it eventually falls into a singularity. If it falls into the singularity, CSCMG is in a state where it cannot perform the desired torque command generation. Therefore, optimal angular momentum vector recovery drive law is required for recovery of the angular momentum vector.

However, another issue to consider is the singularity problem caused by disturbance. There are disturbances caused by wind that interfere with the attitude of the hexarotor. This problem results in fluctuations in the total angular momentum vector. This causes the CMG configuration to easily enter the singular condition, which is similar to the saturation problem of the reaction wheel. Proper use of an internal torquer alone cannot deal with the effects of unwanted external perturbing torque. In this study, Disturbance Robust drive law was proposed. The torque by the hexarotor's motor is appropriately used to overcome the disturbance-based singularity problem. The torque of the CMG and the torque of the motor of the hexarotor are sufficient to prevent entering the singularity due to disturbance. As a result, it is ensured that the external torque can be properly offset and the CMG array can be free from singularity.

A. CMG Mounting Geometry

In this study, a CMG with a relatively simple singularity space as shown in Fig.18 was selected as an actuator for attitude control rather than a pyramidal arrangement commonly used in spacecraft. In the case of an internal/external singularity, it can be divided according to the alignment method of the CMG angular momentum vector as shown in Fig. As shown in Fig.17(a), an internal singularity occurs when the total angular momentum vector of the CMG is zero, and this is when the two CMGs are aligned in opposite directions. As shown in Fig.17(b), an external singularity occurs when the total angular momentum vector has a value twice, which means that the two CMGs are aligned in the same direction. That is, when having such an alignment state, the CMG cannot generate control torque in a desired direction.

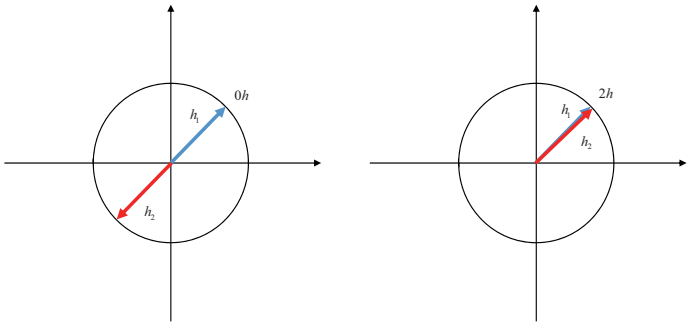

(a) 0h singularity (a) 2h singularity

Figure. 17 Internal/External Singular Conditions of CMGs

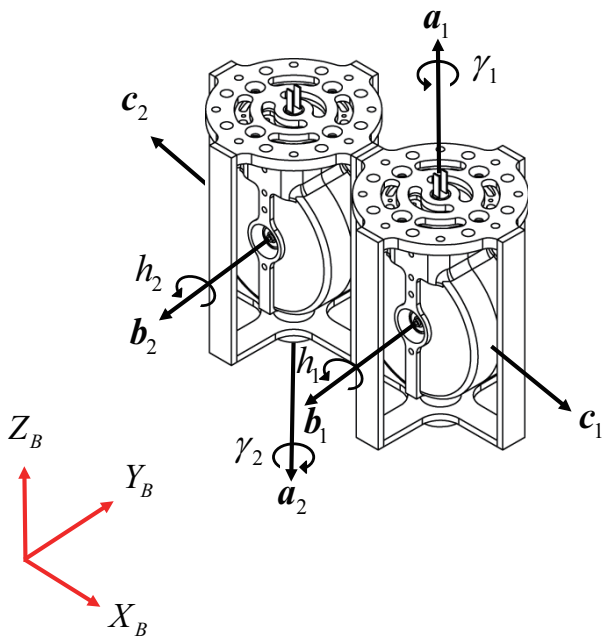

Figure. 18 Two CSCMGs Configuration

B. Pseudo Inverse Drive Law

In order to generate the 3-axis control torque command derived from the control law for the attitude of the hexarotor, the CMG drive law, which is the actuator command distribution law, is required. At this time, the control torque distribution is generally applied using the pseudo inverse drive law. The equation for obtaining the angular velocity vector from the pseudo inverse drive law using the pseudo inverse matrix to evaluate the gimbal angle vector for a given control torque command $\boldsymbol{u}_c$ is as follows.

$$\dot{\boldsymbol{\gamma}} = \mathbf{A}^{\mathbf{T}}\left(\mathbf{A}\mathbf{A}^{\mathbf{T}}\right)^{-1}\boldsymbol{u}_c \tag{61}$$

However, since the Jacobian matrix of the pseudo-inverse drive law is a function of the gimbal angle, there is still the possibility of a singularity occurring for the CMG in a specific gimbal angle arrangement shape.

C. Angular Momentum Vector Recovery Drive Law

The position of the initial gimbal angle is related to the rotational maneuverability of the hexarotor. The angular momentum vector $\boldsymbol{h}_{cmg}$ for the 3 axes is a function of the gimbal angle γ_i, and the value always changes according to the change of the CMG gimbal vector. If one of the most important parts is that the same maneuvering performance should be demonstrated within all maneuvering times, the allowable angular momentum and gimbal operation range for each axis should not be changed before attitude maneuvering begins. That is, it means that the gimbal angle must always return to the initially defined direction. At this time, keep in mind that the gimbal angle must always return to the initial position means that the angular momentum vector must also return to the initial position when the posture maneuver of an arbitrary model ends. If you do not return and gradually move away from the initial value, you will eventually fall into a singularity.

In this study, a Gimbal cector recovery drive law was derived using an optimization technique.

Therefore, the performance index to be minimized was set as follows.

$$\mathcal{J} = \frac{1}{2}\dot{\boldsymbol{\gamma}}^T M \dot{\boldsymbol{\gamma}} + \frac{1}{2}(\dot{\boldsymbol{\gamma}} - \dot{\boldsymbol{\gamma}}_d)^T N\,(\dot{\boldsymbol{\gamma}} - \dot{\boldsymbol{\gamma}}_d) \tag{62}$$

where, M, N is a symmetric positive definite weighting matrix. At this time, we have a constraint equation called $\boldsymbol{u}_c$. The first component of the above equation contributes to minimizing the sum of squares of the control torque input in the same way as the conventional pseudo-inverse matrix. The second component means to find a solution for minimizing the difference between the current angular velocity of the gimbal of the CSCMG gimbal and the angular velocity of the gimbal desired or predetermined by the user.

The desired angular velocity of the gimbal γ_d can be defined as follows.

$$\dot{\boldsymbol{\gamma}}_d = (\boldsymbol{\gamma} - \boldsymbol{\gamma}_d)\,/\Delta t \tag{63}$$

If the optimality condition equation is used to find the optimal solution of Eq.62, the following solution is eventually derived[43].

$$\dot{\boldsymbol{\gamma}} = \mathbf{W}\mathbf{A}^{\mathbf{T}}\left(\mathbf{A}\mathbf{W}\mathbf{A}^{\mathbf{T}}\right)^{-\mathbf{1}}\mathbf{u_c} + \left[\mathbf{W}\mathbf{A}^{\mathbf{T}}\left(\mathbf{A}\mathbf{W}\mathbf{A}^{\mathbf{T}}\right)^{-\mathbf{1}}\mathbf{A}\mathbf{W} - \mathbf{W}\right]\mathbf{g} \tag{64}$$

where, $W = (M+N)^{-1}$, $\boldsymbol{g}$ is non-zero gradient vector, $\boldsymbol{g} = N(\gamma - \gamma_d)/\Delta t$. As a result, it can be seen that the second term on the right hand side is the null vector for momentum vector recovery and the first term is related to the pseudo-inverse drive law.

If the weight matrices M, N are defined as $M = \alpha I_{2\times 2}$ and $N = \beta I_{2\times 2}$, the AMVRSL for obtaining the CSCMG angular acceleration vector can be simply obtained as follows.

$$\dot{\boldsymbol{\gamma}} = \mathbf{A}^{\dagger}\boldsymbol{u}_c + \boldsymbol{n} \tag{65}$$

$$\mathbf{A}^{\dagger} = \mathbf{A}^{\mathbf{T}}\left(\mathbf{A}\mathbf{A}^{\mathbf{T}}\right)^{-1} \tag{66}$$

$$\boldsymbol{n} = \left[\mathbf{A}^{\dagger}\mathbf{A} - \mathbf{I}_{\mathbf{2}\times\mathbf{2}}\right]\varsigma\,(\boldsymbol{\gamma} - \boldsymbol{\gamma}_{\mathbf{d}}) \tag{67}$$

where, $\boldsymbol{n}$ is null vector, α, β are positive constants. GVRSC is activated during the final maneuver section of a redirect mission to any attitude. ς is defined by utilizing the characteristics of the

S-shaped sigmoid function.

$$\varsigma = \frac{\beta}{[(\alpha+\beta)\Delta t]} = \frac{L}{1+e^{-k\sigma}} \tag{68}$$

where, K, L are constants, $\|\boldsymbol{e}\|$ is the norm of the attitude error of the hexarotor, $\|\boldsymbol{\omega}\|$ is the angular velocity vector of the hexarotor and $\sigma = \frac{1}{\|\boldsymbol{e}\|+k_0\|\boldsymbol{\omega}\|} - \varepsilon$. That is, in the final section of the maneuver, both attitude and angular velocity converge to a small value. Therefore, it means that ς is set so that AMVRSL is activated only in the last startup section.

In this study, the angular momentum vector recovery strategy is set to be divided into activation/deactivation according to $\|\boldsymbol{e}\| + \|\boldsymbol{\omega}\| < \upsilon$. If enabled, eta is set to $1/\upsilon = 100$. Also, the maximum value of the null vector is limited from the following standard values.

$$\boldsymbol{n} = \begin{cases} \overline{n}\,\frac{\boldsymbol{n}}{\|\boldsymbol{n}\|_\infty} & , \quad \|\boldsymbol{n}\|_\infty \geq \overline{n} \\ \boldsymbol{n} & , \quad \|\boldsymbol{n}\|_\infty < \overline{n} \end{cases} \tag{69}$$

where, $\|n\|_\infty$ is infinite norm of the generic vector n.

D. Disturbance Robust Drive Law

For During the actual flight of the hexarotor, there are various causes that disturb the attitude of the hexarotor due to wind disturbance. These sources also interfere with the coordination of the CMG, resulting in the singular problem of the array once again. That is, the gimbal does not return to its original position due to external disturbances. It can be seen from the previous case study that the unwanted external disturbance torque cannot be adequately handled using only the torque of the CMG. From now on, the torque of the hexarotor is appropriately used to overcome this disturbance-based singularity problem.

$$\begin{aligned} \mathbf{J}\dot{\boldsymbol{\omega}} + \boldsymbol{\omega}^{\times}\mathbf{J}\boldsymbol{\omega} + \boldsymbol{\omega}^{\times}\boldsymbol{h}_{cmg} &= -\mathbf{A}_{hexa}\boldsymbol{\omega}^2 - \mathbf{A}\left(\gamma\right)\dot{\boldsymbol{\gamma}} + \boldsymbol{d} \\ &= -\mathbf{B}\boldsymbol{u} + \boldsymbol{d} \end{aligned} \tag{70}$$

where,$\boldsymbol{u} = \begin{bmatrix} \boldsymbol{\omega}_i^2 & \dot{\boldsymbol{\gamma}} \end{bmatrix}^T \in R^8$ is the control input. and

$$\mathbf{B} = \begin{bmatrix} \mathbf{A_{hexa}} & \mathbf{A_{cmg}} \end{bmatrix} \in \mathbf{R^{4\times 8}} \tag{71}$$

Through the motion equation of the hexarotor using CMG, it is corrected with a drive law that is strong against disturbance. The optimization problem constrained to minimize the performance index is as follows.

$$\mathcal{J} = \frac{1}{2}\boldsymbol{u}^T\mathbf{P}\boldsymbol{u} + \frac{1}{2}(\boldsymbol{u} - \boldsymbol{u}_d)^T\mathbf{H}\left(\boldsymbol{u} - \boldsymbol{u}_d\right) \tag{72}$$

subject to

$$\boldsymbol{u}_c = \mathbf{B}\boldsymbol{u} \tag{73}$$

where, $\mathbf{P} \in R^{8\times 8}$ and $\mathbf{H} \in R^{8\times 8}$ are the symmetric positive definite weighting matrices. $\boldsymbol{u}_d = \begin{bmatrix} \boldsymbol{\omega}_{i,d}^2 & \dot{\boldsymbol{\gamma}}_d \end{bmatrix}^T \in R^8$ is the desired vector.

By applying the optimal condition[43], the minimum standard solution can be obtained as follows.

$$\boldsymbol{u} = \mathbf{W}\mathbf{B}^{\mathbf{T}}\left(\mathbf{B}\mathbf{W}\mathbf{B}^{\mathbf{T}}\right)^{-1}\boldsymbol{u}_c + \left[\mathbf{W}\mathbf{B}^T\left(\mathbf{B}\mathbf{W}\mathbf{B}^T\right)^{-1}\mathbf{B}\mathbf{W} - \mathbf{W}\right]\boldsymbol{g} \tag{74}$$

where, $\mathbf{W}$, $\boldsymbol{g}$ are the gradient vector forcing the gimbal angle to the preferred original position,

P and **H** are weighting matrices.

Since there are many solutions that satisfy Eq.71, the pseudo-inverse solution to the first term on the right hand side of Eq.74 is the most advantageous choice. It is simply rewritten as

$$\boldsymbol{u} = \mathbf{A}^T\left(\mathbf{A}\mathbf{A}^T\right)^{-1}\boldsymbol{u}_c + \boldsymbol{n} \tag{75}$$

$$\boldsymbol{n} = \left[\mathbf{W}\mathbf{B}^T\left(\mathbf{B}\mathbf{W}\mathbf{B}^T\right)^{-1}\mathbf{B}\mathbf{W} - \mathbf{W}\right]\varsigma\left(\boldsymbol{u} - \boldsymbol{u}_d\right) \tag{76}$$

where, $\boldsymbol{n}$ is the null vector

and

$$\begin{aligned}
&\boldsymbol{u}_c = \mathbf{B}\boldsymbol{u} \in R^4 \\
&\mathbf{B} = \begin{bmatrix} \mathbf{A}_{hexa} & \mathbf{A}_{cmg} \end{bmatrix} \in R^{4\times 8} \\
&\mathbf{A}_{hexa} \in R^{4\times 6} \\
&\mathbf{A}_{cmg} \in R^{4\times 2} \\
&\boldsymbol{u} = \begin{bmatrix} \boldsymbol{\omega}_i^2 & \dot{\boldsymbol{\gamma}} \end{bmatrix}^T \in R^8 \\
&\boldsymbol{u}_d = \begin{bmatrix} \boldsymbol{\omega}_{i,d}^2 & \dot{\boldsymbol{\gamma}}_d \end{bmatrix}^T \in R^8 \\
&\mathbf{P} = \begin{bmatrix} p_{hexa}\mathbf{I}_{6\times 6} & \mathbf{O}_{6\times 2} \\ \mathbf{O}_{2\times 6} & p_{cmg}\mathbf{I}_{2\times 2} \end{bmatrix} \in R^{8\times 8} \\
&\mathbf{H} = \begin{bmatrix} q_{hexa}\mathbf{I}_{6\times 6} & \mathbf{O}_{6\times 2} \\ \mathbf{O}_{2\times 6} & q_{cmg}\mathbf{I}_{2\times 2} \end{bmatrix} \in R^{8\times 8} \\
&\mathbf{W} = (\mathbf{P} + \mathbf{H})^{-1} \in R^{8\times 8} \\
&\boldsymbol{g} = \mathbf{H}\left(\boldsymbol{u} - \boldsymbol{u}_d\right) \in R^7
\end{aligned} \tag{77}$$

where $0_{m\times n}$ denotes the $m \times n$ zero matrix and p_{hexa}, p_{cmg}, q_{hexa}, and q_{cmg} are the weighting constants.

E. Numerical Simulation

1. Simulation Configuration

Numerical simulation related to drive law is performed. The block diagram of the designed system according to the drive law is shown in Fig.19. In order to perform the maximum maneuver of the hexarotor with two CSCMGs, the simulation was conducted under the conditions shown in Table.3. The drive law to derive the angular velocity value of the CSCMG gimbal was compared and analyzed by applying the Pseudo Inverse drive law and the disturbance robust drive law. Parameters of DRSL are shown in Table.4. The disturbance scenario was designed with the torque value as shown in Fig. 10, and the simulation was conducted by adding the external torque value to the modeling formula of the hexarotor.

Table 3: Simulation configuration conditions

Parameter	Values	Parameter	Values
Number of commands	30	Total time (sec)	600
One command time (sec)	20	Command maximum (deg)	±30

Table 4: Simulation parameters of DRSL

Parameter	Values	Parameter	Values
L	1	p_{hexa}	1e5
k_0	1	q_{hexa}	1e5
k	1	p_{cmg}	10
ε	500	q_{cmg}	1
$\overline{n}$	0.1		

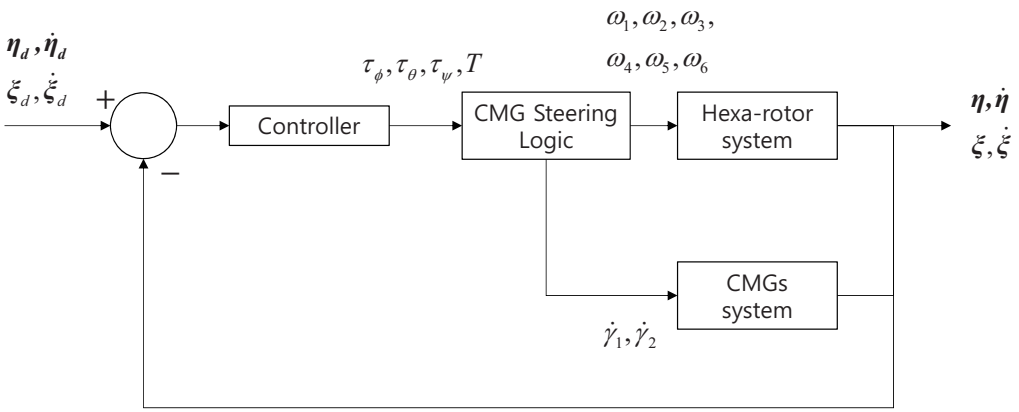

Figure. 19 Block Diagram of System of Hexarotor with CMGs

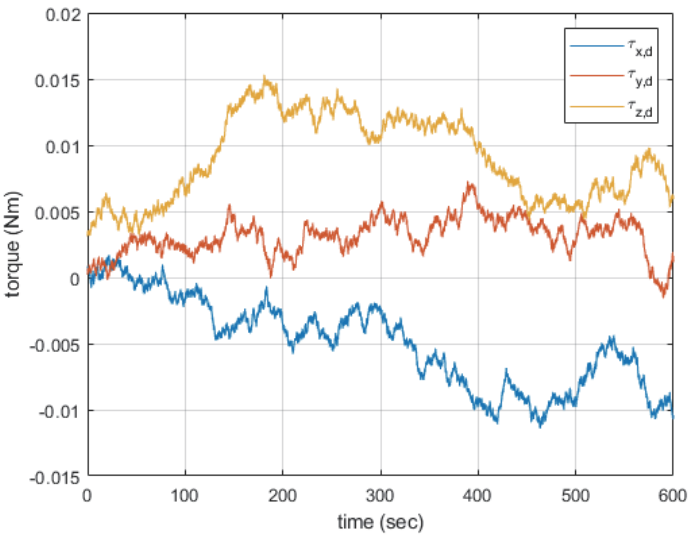

Figure. 20 Disturbance Scenario

2. Pseudo Inverse Drive Law Simulation Result

Figure.21-25 is a state graph of a hexarotor with CMG in an environment with disturbance by pseudo inverse drive law. Figure.21 is the attitude state controlled by multiple attitude commands. There are some errors due to disturbance, but it can be confirmed that all of them converge to the target attitude. Figure.22 and 23 are the motor speed and torque graphs of the hexarotor. It can be seen that the shaking phenomenon appears during posture command conversion. This phenomenon is caused by the sign function in the arrival law and is called chattering. Figure.24 is the angle graph of the CMG gimbal. The initial gimbal angle was set at 45 deg. After a few minutes, you can see that the initial gimbal angle and the error gradually develop. This means that the gimbal cannot be restored to its initial angle due to disturbance. Figure.25 is the angular velocity graph of the CMG gimbal. Angular velocity of the gimbal chatter within hardware limits. It was confirmed that the hexarotor with CMG using pseudo inverse drive law could not accurately generate the necessary control torque commands in a disturbance environment.

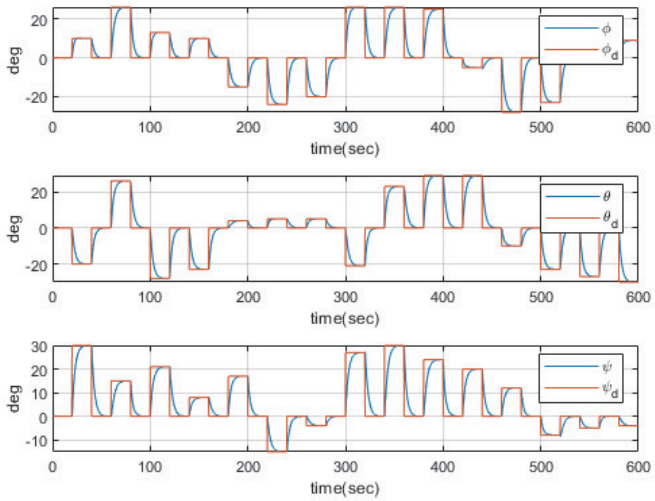

Figure. 21 Histories of Attitude of Hexarotor with Disturbances

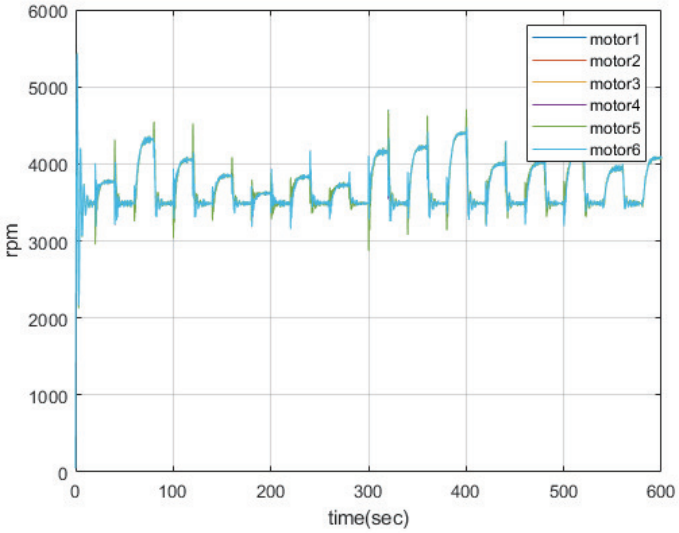

Figure. 22 Histories of Motor Speed of Hexarotor with Disturbances

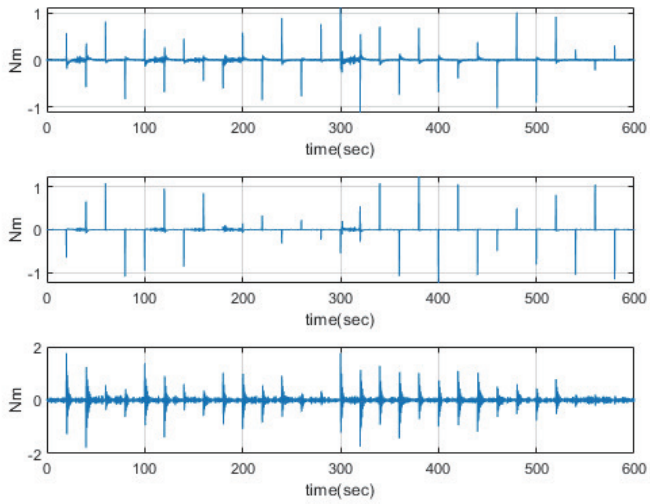

Figure. 23 Histories of Torque of Hexarotor with Disturbances

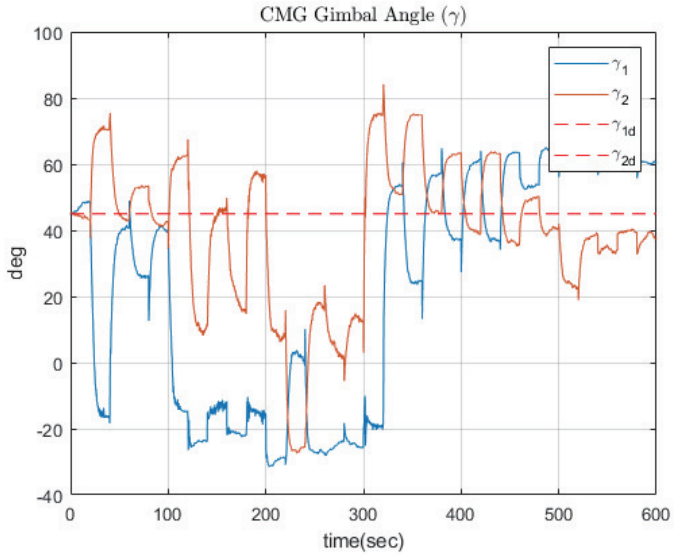

Figure. 24 Histories of Gimbal Angle of Hexarotor with Disturbances

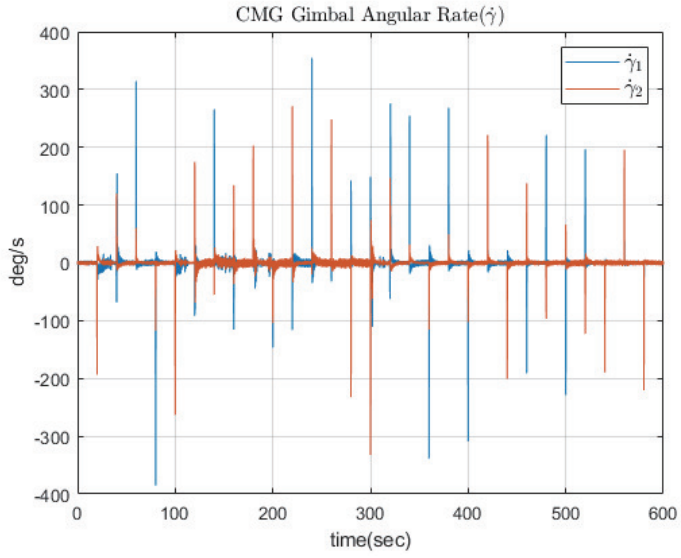

Figure. 25 Histories of Gimbal Rate of Hexarotor with Disturbances

3. Disturbance Robust Drive Law Simulation Result

Figure.26-30 is a state graph of a hexarotor with CMG in a disturbance environment by disturbance robust drive law. Figure 26 is the attitude state controlled by multiple attitude commands. There are some errors due to disturbance, but it can be confirmed that all of them converge to the target attitude. Figure.27 and 28 are the motor speed and torque graphs of the hexarotor. It can be seen that the shaking phenomenon appears during posture command conversion. This phenomenon is caused by the sign function in the arrival law and is called chattering. Figure.29 is the angle graph of the CMG gimbal. The initial gimbal angle was set at 45 deg. It was confirmed that the gimbal angle is much more stable during multi-attitude command maneuvers than in the case of pseudo inverse drive law. Figure.30 is the angular velocity graph of the CMG gimbal. It was confirmed that the angular velocities of the gimbal of the two CMGs were also very stable within hardware limits. It was confirmed that the hexarotor with CMG using the disturbance robust drive law does not cause the singularity problem and avoids it even in the environment with disturbance. Therefore, it was confirmed that the disturbance robust drive law does not fall into the singularity problem and performs a stable CMG operation against disturbance.

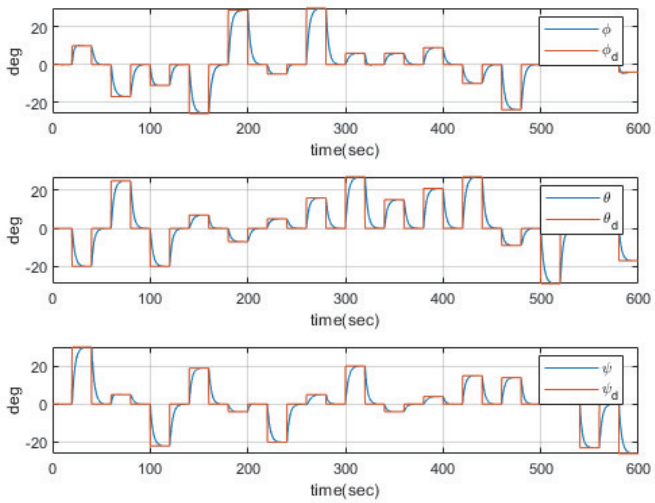

Figure. 26 Histories of Attitude of Hexarotor with Disturbances

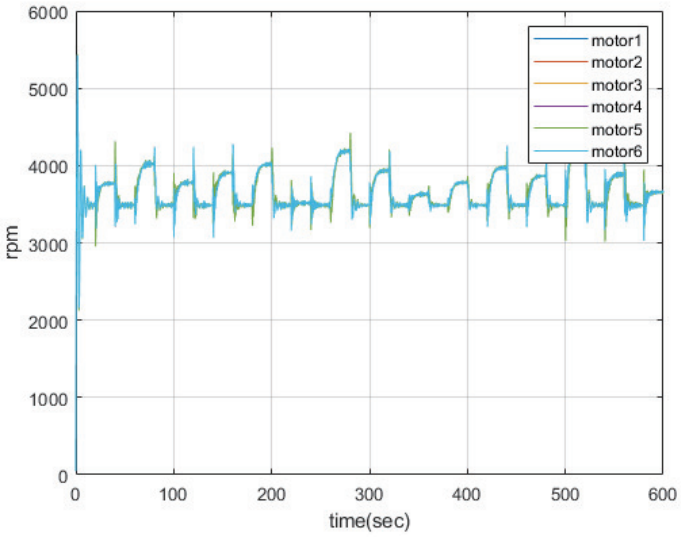

Figure. 27 Histories of Motor Speed of Hexarotor with Disturbances

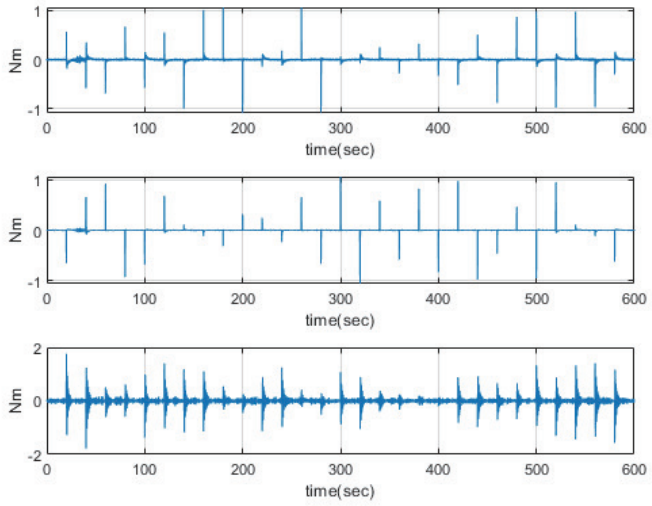

Figure. 28 Histories of Torque of Hexarotor with Disturbances

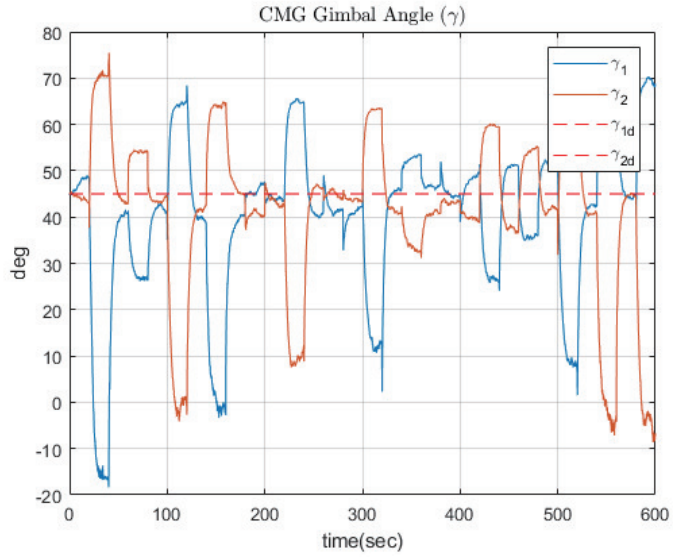

Figure. 29 Histories of Gimbal Angle of Hexarotor with Disturbances

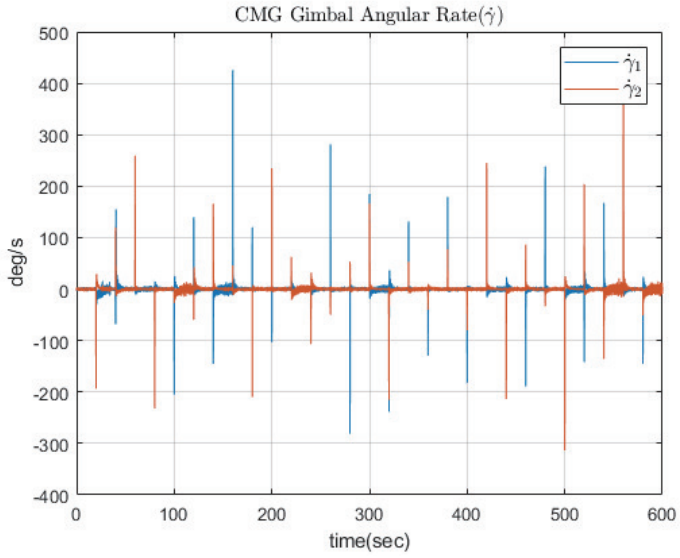

Figure. 30 Histories of Gimbal Rate of Hexarotor with Disturbances

VI. Conclusion

Recently, stability and reliability are very important as multi-rotors perform various missions replacing human resources. In order to perform the mission more effectively, three solutions are suggested.

In order to ensure flight stability and reliability, sliding mode control, which is a representative nonlinear model control technique, is applied, and disturbances such as wind or model uncertainty can be resolved. However, FTSMC was applied to solve the problem of general SMC, that it takes infinite time for the state error to converge to 0.

Since it is difficult to guarantee attitude stability through speed control only with the rotor of a multi-rotor in a large disturbance, a CMG actuator is proposed to ensure attitude stability with a fast response speed. Since two CSCMGs are installed on the multi-rotor, the problem of not guaranteeing flight stability through speed control with only the rotors of the multi-rotor against external disturbances has been solved.

Finally, a driving law is presented to overcome the singularity of CMG. It is very important for CMG to restore the initial gimbal angle. In this paper, DRSL is presented to overcome the singularity problem caused by disturbance.

Therefore, it was confirmed that the multi-rotor with CMG can overcome the singularity problem and ensure flight stability and reliability in the environment with disturbance.

Through this study, it is expected that it will be helpful for research such as multi-rotor landing on a ship by improving the performance of the multi-rotor for more stable attitude control, hovering, and high maneuverability such as fast command-following.

References

[1] X. Wang, Z. Huang, G. Sui, H. Lian *et al.*, "Analysis on the development trend of future uav equipment technology," *Academic Journal of Engineering and Technology Science*, vol. 2, no. 1, 2019.

[2] H. Menouar, I. Guvenc, K. Akkaya, A. S. Uluagac, A. Kadri, and A. Tuncer, "Uav-enabled intelligent transportation systems for the smart city: Applications and challenges," *IEEE Communications Magazine*, vol. 55, no. 3, pp. 22–28, 2017.

[3] J.-K. Park, A. Das, and J.-H. Park, "Application trend of unmanned aerial vehicle (uav) image in agricultural sector: Review and proposal," *Korean Journal of Agricultural Science*, vol. 42, no. 3, pp. 269–276, 2015.

[4] D. Ventura, M. Bruno, G. J. Lasinio, A. Belluscio, and G. Ardizzone, "A low-cost drone based application for identifying and mapping of coastal fish nursery grounds," *Estuarine, Coastal and Shelf Science*, vol. 171, pp. 85–98, 2016.

[5] H. Shakhatreh, A. H. Sawalmeh, A. Al-Fuqaha, Z. Dou, E. Almaita, I. Khalil, N. S. Othman, A. Khreishah, and M. Guizani, "Unmanned aerial vehicles (uavs): A survey on civil applications and key research challenges," *Ieee Access*, vol. 7, pp. 48 572–48 634, 2019.

[6] K. F. A. Lab, "Domestic and foreign drone industry trends analysis report," *KIAST*, 2021.

[7] P. S. T. of the Safety Monitoring Bureau, "Drone safety status survey results," *Korea Consumer Agency*, 2017.

[8] G. V. Raffo, M. G. Ortega, and F. R. Rubio, "An integral predictive/nonlinear h∞ control structure for a quadrotor helicopter," *Automatica*, vol. 46, no. 1, pp. 29–39, 2010.

[9] S. Islam, P. X. Liu, and A. El Saddik, "Robust control of four-rotor unmanned aerial vehicle with disturbance uncertainty," *IEEE Transactions on Industrial Electronics*, vol. 62, no. 3, pp. 1563–1571, 2014.

[10] R. Xu and U. Ozguner, "Sliding mode control of a quadrotor helicopter," in *Proceedings of the 45th IEEE Conference on Decision and Control*. IEEE, 2006, pp. 4957–4962.

[11] T. Madani and A. Benallegue, "Backstepping control for a quadrotor helicopter," in *2006 IEEE/RSJ International Conference on Intelligent Robots and Systems*. IEEE, 2006, pp. 3255–3260.

[12] C. Nicol, C. Macnab, and A. Ramirez-Serrano, "Robust neural network control of a quadrotor helicopter," in *2008 Canadian conference on electrical and computer engineering*. IEEE, 2008, pp. 001 233–001 238.

[13] Y. Shtessel, C. Edwards, L. Fridman, A. Levant *et al.*, *Sliding mode control and observation*. Springer, 2014, vol. 10.

[14] M.-L. Tseng and M.-S. Chen, "Chattering reduction of sliding mode control by low-pass filtering the control signal," *Asian Journal of control*, vol. 12, no. 3, pp. 392–398, 2010.

[15] J. L. Hernandez, I. González-Hernández, and R. Lozano, "Super-twisting control in a solar unmanned aerial vehicle: Application to solar tracking," in *2018 International Conference on Unmanned Aircraft Systems (ICUAS)*. IEEE, 2018, pp. 379–384.

[16] A. Mehta and B. Bandyopadhyay, *Frequency-shaped and observer-based discrete-time sliding mode control*. Springer, 2015.

[17] R. Fessi, S. Bouallègue, J. Haggège, and S. Vaidyanathan, "Terminal sliding mode controller design for a quadrotor unmanned aerial vehicle," in *Applications of sliding mode control in science and engineering*. Springer, 2017, pp. 81–98.

[18] X. Yu and M. Zhihong, "Fast terminal sliding-mode control design for nonlinear dynamical systems," *IEEE Transactions on Circuits and Systems I: Fundamental Theory and Applications*, vol. 49, no. 2, pp. 261–264, 2002.

[19] J.-J. Xiong and E.-H. Zheng, "Position and attitude tracking control for a quadrotor uav," *ISA transactions*, vol. 53, no. 3, pp. 725–731, 2014.

[20] H. Leeghim, C.-Y. Lee, J. Jin, and D. Kim, "A singularity-free steering law of roof array of control moment gyros for agile spacecraft maneuver," *International Journal of Control, Automation and Systems*, vol. 18, no. 7, pp. 1679–1690, 2020.

[21] I. Jikuya, K. Fujii, and K. Yamada, "Attitude maneuver of spacecraft with a variable-speed double-gimbal control moment gyro," *Advances in Space Research*, vol. 58, no. 7, pp. 1303–1317, 2016.

[22] Y.-H. Wu, F. Han, M.-H. Zheng, F. Wang, B. Hua, Z.-M. Chen, and Y.-H. Cheng, "Attitude tracking control for a space moving target with high dynamic performance using hybrid actuator," *Aerospace Science and Technology*, vol. 78, pp. 102–117, 2018.

[23] S.-H. Mok, H. Bang, and H.-S. Kim, "Analytical solution for attitude command generation of agile spacecraft," *Journal of the Korean Society for Aeronautical & Space Sciences*, vol. 46, no. 8, pp. 639–651, 2018.

[24] H. Lee, D. Lee, and H. Bang, "Hybrid control of spacecraft using various momentum exchange devices," in *The 5th Asian Control Conference, Bali, Indonesia*, 2006.

[25] H. Leeghim, "Optimal steering laws for control moment gyros," *Korea Advanced Institute of Science and Technology, Doctoral Dissertation*, 2007.

[26] H. Schaub, S. R. Vadali, and J. L. Junkins, "Feedback control law for variable speed control moment gyros," *The Journal of the astronautical sciences*, vol. 46, no. 3, pp. 307–328, 1998.

[27] S.-h. Jang and H. Leeghim, "Nonlinear attitude control of drones using control moment gyros," *Journal of the Korean Society for Aeronautical & Space Sciences*, vol. 49, no. 10, pp. 821–828, 2021.

[28] Y. Kgim and H. Leeghim, "Drone control using control moment gyro," in *Proceeding of The Korean Society for Aeronautical and Space Sciences Fall Conference*, 2016, pp. 917–919.

[29] D. Maloney, "Reaction wheels almost control this unusual drone," *Hackaday*, 2019.

[30] C. Gulcen, "Uav using internal momentum wheels," *Master Thesis, Cranfield University*, 2017.

[31] H. Leeghim and D. Kim, "Singularity-robust control moment gyro allocation strategy for spacecraft attitude control in the presence of disturbances," *Aerospace Science and Technology*, vol. 119, p. 107178, 2021.

[32] B. Wie, "Singularity escape/avoidance steering logic for control moment gyro systems," *Journal of guidance, control, and dynamics*, vol. 28, no. 5, pp. 948–956, 2005.

[33] H. Schaub and J. L. Junkins, "Singularity avoidance using null motion and variable-speed control moment gyros," *Journal of Guidance, Control, and Dynamics*, vol. 23, no. 1, pp. 11–16, 2000.

[34] H. Leeghim, H. Bang, and J.-O. Park, "Singularity avoidance of control moment gyros by one-step ahead singularity index," *Acta Astronautica*, vol. 64, no. 9-10, pp. 935–945, 2009.

[35] Y. Nakamura and H. Hanafusa, "Inverse kinematic solutions with singularity robustness for robot manipulator control," 1986.

[36] A. Alaimo, V. Artale, C. Milazzo, A. Ricciardello, and L. Trefiletti, "Mathematical modeling and control of a hexacopter," in *2013 International Conference on Unmanned Aircraft Systems (ICUAS)*. IEEE, 2013, pp. 1043–1050.

[37] V. Artale, C. Milazzo, and A. Ricciardello, "Mathematical modeling of hexacopter," *Applied mathematical sciences*, vol. 7, no. 97, pp. 4805–4811, 2013.

[38] R. Leishman, J. Macdonald, T. McLain, and R. Beard, "Relative navigation and control of a hexacopter," in *2012 IEEE International Conference on Robotics and Automation*. IEEE, 2012, pp. 4937–4942.

[39] J. G.-A. J.M. Rico-Martinez, "A simple method for the determination of angular velocity and acceleration of a spherical motion through quaternions," *Meccanica*, 2000.

[40] T. Luukkonen, "Modelling and control of quadcopter," *Independent research project in applied mathematics, Espoo*, vol. 22, p. 22, 2011.

[41] H. Yoon and P. Tsiotras, "Spacecraft adaptive attitude and power tracking with variable speed control moment gyroscopes," *Journal of Guidance, Control, and Dynamics*, vol. 25, no. 6, pp. 1081–1090, 2002.

[42] J. Wang, K. A. Alattas, Y. Bouteraa, O. Mofid, and S. Mobayen, "Adaptive finite-time backstepping control tracker for quadrotor uav with model uncertainty and external disturbance," *Aerospace Science and Technology*, p. 108088, 2022.

[43] A. E. Bryson and Y.-C. Ho, *Applied optimal control: optimization, estimation, and control*. Routledge, 2018.